Lithos 318–319 (2018) 326–339

Contents lists available at ScienceDirect

Lithos

journal homepage: www.elsevier.com/locate/lithos

Magmatic-tectonic control on the generation of silicic magmas in Iceland: Constraints from Hafnarfjall-Skarðsheiði volcano

Tenley J. Banik [a,*], Calvin F. Miller [a], Christopher M. Fisher [b], Matthew A. Coble [c], Jeffrey D. Vervoort [b]

[a] Dept. of Earth and Environmental Sciences, Vanderbilt University, Nashville, TN 37240, USA
[b] School of the Environment, Washington State University, Pullman, WA 99164, USA
[c] Stanford University, Geological Sciences Dept., Stanford, CA 94305, USA

ARTICLE INFO

Article history:
Received 12 May 2018
Accepted 15 August 2018
Available online 20 August 2018

ABSTRACT

Hafnarfjall-Skarðsheiði (H-S) central volcano, located at the edge of the Western rift zone in Iceland, provides a snapshot into silicic magma generation that occurred soon after establishment of a rift. We present in situ zircon U-Pb ages and oxygen and hafnium isotope compositions, complemented by whole-rock major and trace element and Pb, Nd, and Hf whole rock isotope data, from the dominant silicic units erupted throughout H-S's eruptive history. Zircon U-Pb ages (ca. 5.4 to 3.9 Ma) and field relationships indicate silicic magmatism was episodic. However, relatively low (for Iceland) whole rock ε_{Hf} (+11.9 to 13.3) and ε_{Nd} (+7.2 to 7.6), in addition to Pb isotope data from basalt and rhyolite units indicate that the same mantle-derived source is dominantly responsible for the geochemical characteristics observed in both magma types, which are more similar to those from magmas from a propagating rift than an established one. This observation is consistent with a role for fractional crystallization of mantle melts in addition to contributions of partially melted altered crust to explain the low $\delta^{18}O_{zrc}$ values (1.5 to 4.6‰) observed. This study highlights the importance of the evolutionary state of the rift, crustal history, and mantle heterogeneity all as contributing factors to the isotopic composition of silicic Icelandic magmas. We invoke a petrogenetic model where the timescales of rift drift explain the long-lived, episodic silicic magmatism produced during rift propagation at Hafnarfjall-Skarðsheiði volcano.

1. Introduction

On Iceland, an active mid-ocean ridge and a major mantle plume coincide to produce an island plateau where silicic ($SiO_2 \geq 65$ wt%) rocks are abundant (~10–15% of exposed rocks; e.g. Jónasson, 2007; Thorarinsson, 1967; Walker, 1966) compared to typical oceanic crust. Petrogenesis of the silicic magmas from which these rocks formed has long stimulated interest and debate, in part because of their unique abundance and speculation about their implications for early continental crust formation (e.g. Willbold et al., 2009; Reimink et al., 2014; cf. Martin et al., 2008; Carley et al., 2014). Current models for silicic magma petrogenesis in Iceland invoke partial melting of hydrothermally altered crust (e.g. Bindeman et al., 2012; Gunnarsson et al., 1998; Jónasson, 1994; Marsh et al., 1991; Óskarsson et al., 1982; Sigmarsson et al., 1991), fractional crystallization of primary basaltic magma (e.g. Carmichael, 1964; Furman et al., 1992; Macdonald et al., 1987; Nicholson et al., 1991; Prestvik et al., 2001), and both processes, either independently or acting in tandem (e.g. Martin and Sigmarsson, 2010; Sigmarsson et al., 1992a, 1992b). These studies provide constraints on magmatic processes in Iceland, but they often do not consider the specific tectonic history and environment in which each volcano's silicic magmas are produced. Given the unique geodynamic setting in which Icelandic rhyolites are generated, effects of rifting should be taken into account when addressing processes and timescales associated with their petrogenesis.

The Mid-Atlantic Ridge and Iceland plume became coupled roughly 25 Ma, which led to abnormally high rates of magma production and continuously constructed the thick Icelandic crust (25–40 km; e.g. Bjarnason, 2008; Brandsdóttir and Menke, 2008). As a result of ridge/plume coupling and northwestern drift of the ridge axis, the Mid-Atlantic Ridge around Iceland—exposed on land as a series of rift zones—deviates progressively east of the main ridge axis to remain coupled with the plume. The plume periodically recaptures the ridge through a rift relocation, which effectively moves the rift eastward through time (Harðarson et al., 2008). Rift relocations have occurred several times throughout Iceland's approximately 20 Myr history. Field relationships, including unconformities in sedimentary sequences (e.g. Sæmundsson, 1974) and synclinal structures in the basalt succession (e.g. Jóhannesson, 1980; Óskarsson et al., 1985; Sæmundsson, 1967; Vink, 1984), along with paleomagnetic and geochemical data, are invoked to identify formerly active segments of the main rift axis prior to the initiation of the currently active Western and Northern rift zones (WRZ

* Corresponding author at: Dept. of Geography, Geology, and the Environment, Illinois State University, Normal, IL 61790, USA.
E-mail address: tjbanik@ilstu.edu (T.J. Banik).

https://doi.org/10.1016/j.lithos.2018.08.022
0024-4937/

and NRZ), propagating Eastern rift zone (ERZ) and their corresponding Volcanic Zones (WVZ, NVZ, and EVZ, respectively; Fig. 1) (e.g. Harðarson et al., 2008). The Snæfellsnes-Skagi rift zone (SSRZ) became extinct between 6.7 and 5.5 Ma at which time the main rift and volcanic activity in the southwest of Iceland transferred to the WRZ. Silicic magmas are generated during dynamic processes of rift relocation (e.g. Hardarson et al., 1997, and many others), but ascertaining the mechanisms by which they form in such a setting is complicated by uncertainties surrounding involvement of pre-existing crust and the timescales on which silicic magmas form after a rift relocation.

Hafnarfjall-Skarðsheiði volcano (H-S) began forming nearly contemporaneously with the SSRZ-to-WRZ rift relocation and provides an excellent opportunity to study the timescales and processes associated with silicic petrogenesis, particularly those processes related to tectonic control. H-S is one of the few areas in Iceland with appreciable silicic material erupted soon after its parent rift relocated. H-S unconformably overlies crust generated in the SSRZ that contains no evidence of other propagating rifts or faults to complicate the interpretation of the underlying crustal material. Prior research by Franzson (1978), Gautneb et al. (1989), and Browning and Gudmundsson (2015), along with a series of regional paleomagnetic ages, provides a detailed petrologic and geophysical framework in which to place our findings. Franzson (1978) largely focused on the petrogenesis of the volumetrically dominant basaltic units in the H-S volcanic complex and the regional tectonics, but speculated that the silicic rocks formed predominantly by partial melting of the lower crust without undertaking further investigation into silicic magma genesis and rift relocation.

We use zircon and whole rock elemental and isotope geochemistry to investigate the development of silicic magmas at the Hafnarfjall-Skarðsheiði central volcano and evaluate the interactions of rift relocation, spreading, and silicic magmatism. Studies in Iceland that incorporate zircon data have focused on historically active volcanoes (Carley et al., 2011), Tertiary intrusions in east Iceland (Padilla et al., 2016), and Tertiary detrital samples (Carley et al., 2017). The results presented here constitute the first comprehensive zircon-based, whole rock-supported study of silicic petrogenesis at a central volcano conducted in western Iceland. Based on this new data set, we propose a refined interpretation of the interplay between tectonics and silicic petrogenesis and the timing of silicic magma production after rift relocation.

2. Background and sampling of Hafnarfjall-Skarðsheiði

2.1. Geologic setting of Hafnarfjall-Skarðheiði

H-S is an eroded central volcano located in western Iceland (Fig. 1), at the western edge of the Western Volcanic Zone (WVZ). H-S erupted from the currently active Western Rift Zone (WRZ) between ~6 and 4 Ma, early in the rift's active history (Franzson, 1978; Harðarson et al., 2008; Moorbath et al., 1968). It is a well-preserved example of a multi-caldera central volcano constructed of numerous basaltic sheets and approximately ten silicic units (Supplemental Table S6). The majority of the silicic units are volcanic, with one granophyric unit, but in total account for ~20 area% of the succession and erupted throughout the volcano's lifetime (Franzson, 1978). Prior regional field reconnaissance, mapping, and sampling by Franzson (1972, 1978, the reader is referred to these studies for a detailed description of the study area) revealed tholeiitic basalts at the base of the succession that lie unconformably on olivine tholeiite and porphyritic tholeiite basalts that predate the H-S central volcano by several million years (up to ~10–13 Ma). Silicic magmas first appeared in the early stages of central volcano-forming activity in Brekkufjall (Fig. 1) and erupted intermittently before and after an early caldera collapse. The focus of eruptive activity then shifted southwest toward Hafnarfjall (Fig. 1), resulting in a series of flood basalts that pre-dated the main Hafnarfjall caldera. Browning and Gudmundsson (2015) suggest that the edifice of the Hafnarfjall central volcano was over 1000 m in elevation prior to caldera collapse. Franzson (1978) described a large collapse event at ca. 4.6 Ma that resulted in a ~7.5 × 5 km caldera in Hafnarfjall and vertical displacement of over 200 m (Browning and Gudmundsson, 2015). However, the lack of identified extensive silicic lavas or outflow ignimbrite deposits

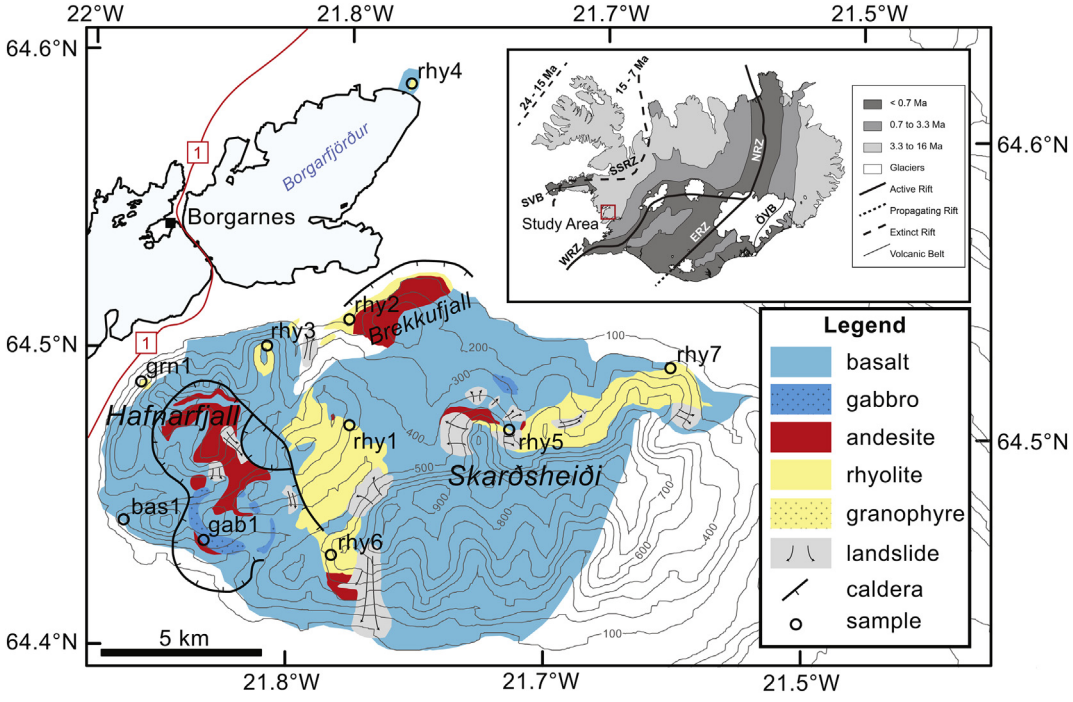

Fig. 1. Geologic maps of Iceland and Hafnarfjall-Skarðsheiði. (inset) General geologic map of Iceland showing active and extinct rift axes and ages of bedrock sourced from each. Location of Hafnarfjall-Skarðsheiði volcano is in the red box on west coast. Snæfellsnes-Skagi rift zone (SSRZ), Western, Eastern, and Northern rift zones (WRZ, ERZ, NRZ), Snæfellsness volcanic belt (SVB), and Öræfi volancic belt (ÖVB) shown for reference. Modified after Harðarson (2008). (main) Generalized geologic map of Hafnafjall-Skarðsheiði central volcano with sample locations (rhy1–7; grn1; gab1; bas1). Modified from Franzson (1978) and Browning et al., (2015).

of this age surrounding the caldera suggests the involvement of basalt lavas in caldera collapse. Formation of the Hafnarfjall caldera led to emplacement of several small-volume silicic plugs around the eastern margin of the caldera and extensive basaltic and andesitic activity within the central portion of the caldera. After the Hafnarfjall caldera-forming event, the focus of volcanic activity shifted east, producing an extensive series of silicic and intermediate flows, domes, and ignimbrites in Skarðsheidi. The final magmatic activity at H-S consisted of dominantly basalt and andesite flows and several shallow intrusions, including at least one gabbro and the only silicic intrusion in the complex—the 3.9 ± 0.6 Ma (whole rock K-Ar age) Flyðrur granophyre (Moorbath et al., 1968). The extinction of the central volcano occurred roughly at this time, but basaltic lavas continued to erupt intermittently around the southeastern margin of the volcano (Franzson, 1978).

2.2. Samples studied

We sampled seven silicic units (six volcanic and one intrusive), one related silicic volcanic unit several km north of the central volcano, and two mafic units—a tholeiitic basalt from the Hafnarfjall phase and a late-stage gabbro interpreted to be a cumulate (Fig. 1, Table 1)—in order to document the longevity and geochemical characteristics of the silicic magmatic system. While we sampled the freshest rocks available from major silicic outcrops identified from the geologic map of Franzson (1978), the majority of the units in the central volcano are altered, which may compromise whole rock major and fluid-mobile trace element concentrations. Zircon is strongly resistant to chemical weathering (e.g. Hoskin and Schaltegger, 2003; Valley, 2003) compared to whole rock samples and therefore provides a more robust measure of the original melt composition—particularly for isotopic compositions—from which zircon crystallized.

3. Analytical techniques

3.1. Whole rock analyses

Major element whole rock compositions were determined using X-ray fluorescence (XRF) at the Geoanalytical Laboratory at Washington State University using the methods of Johnson et al. (1999). Whole rock trace-element abundances were determined using both XRF and ICP-MS via standard techniques. Analytical precision for XRF analyses is listed in Supplemental Table S9. Relative precision for ICP-MS analyses is typically better than 5% for the REEs and 10% for the remaining trace elements. Whole rock Nd, Hf, and Pb isotope compositions were measured at the Radiogenic Isotope and Geochronology Laboratory at Washington State University using the procedure outlined in McDowell et al. (2016). Isotope compositions were measured on a Thermo-Finnigan Neptune MC-ICP-MS. Whole rock Hf isotope analyses were corrected for mass fractionation using $^{179}Hf/^{177}Hf = 0.7325$ and normalized using Hf standard JMC475 ($^{176}Hf/^{177}Hf = 0.282160$; Vervoort and Blichert-Toft, 1999). The measured JMC-475 $^{176}Hf/^{177}Hf$ ratio was 0.282132 ± 0.000007 (2σ standard deviation (SD)), which resulted in a correction factor of 1.000093. Nd isotope analyses were corrected for mass fractionation using $^{146}Nd/^{144}Nd = 0.7219$ and normalized using a correction factor of 1.000052 based on measurements of La Jolla Nd standard ($^{143}Nd/^{144}Nd = 0.51185$, Lugmair et al., 1983); our value was 0.511831 ± 0.000014 (2σ SD). We corrected for mass bias in the whole rock Pb isotope analyses using $^{205}Tl/^{203}Tl = 2.388$ and normalized the mass bias corrected values for standard NBS 981 using $^{206}Pb/^{204}Pb = 16.9405$, $^{207}Pb/^{204}Pb = 15.4963$, $^{208}Pb/^{204}Pb = 36.7219$ (Galer and Abouchami, 1998). Our measured NBS 981 values, with 2σ SD, were: $^{206}Pb/^{204}Pb = 16.9361 \pm 0.0010$, $^{207}Pb/^{204}Pb = 15.4924 \pm 0.0008$, and $^{208}Pb/^{204}Pb = 36.7016 \pm 0.0018$.

3.2. Zircon analyses

Zircons were separated from nine H-S rock samples using standard crushing, sieving, and magnetic and density separation techniques, followed by hand picking. Zircon grains were mounted in epoxy, polished to expose grain interiors, and imaged using the Vanderbilt University EES Tescan Vega 3 LM variable pressure scanning electron microscope using cathodoluminescence (CL) and backscattered electron imaging prior to analysis. Grains selected for analysis were filtered to avoid obvious surface impurities and identify potential inheritance and zoning diversity (Supplemental Fig. S1).

We performed 152 oxygen isotope analyses at the University of California–Los Angeles National Science Foundation CAMECA ims-1270 secondary ion mass spectrometer following the methods of Trail et al. (2007). Operating conditions include a Cs^+ primary ion beam with an analytical spot size of ~20–25 μm and analytical pit depth of ~1 μm. Measured ratios were corrected for mass discrimination using primary zircon standard R33 ($\delta^{18}O = 5.55 \pm 0.08‰$ (2SD); Valley, 2003) and all data are reported as $\delta^{18}O$ calculated relative to VSMOW of Baertschi (1976). Cited precisions are 2σ uncertainties (calculated in quadrature using both the analytical uncertainty of individual analyses and the external reproducibility of standards). External 1σ reproducibility for R33 analyses ranged from 0.29 to 0.42 (see Supplemental Table S1).

Zircon U/Pb ages and trace element compositions were obtained using the sensitive high-resolution ion microprobe with reverse geometry (SHRIMP-RG) jointly operated by the U.S. Geological Survey and Stanford University. Zircon mounts were lightly polished to remove O isotope analytical pits prior to analysis and re-imaged via CL. Operating procedure included an O_2^- primary ion beam focused to a ~25 × 17 μm diameter analytical spot for U-Pb isotopes and ~12 × 12 μm diameter for trace element analyses. Zircons from three samples (rhy1, rhy4, and rhy5) were analyzed using a routine that combined U-Pb age and a limited number of trace elements using a ~25 × 25 μm analytical spot (Supplemental Table S3). U-Pb ages were calibrated using zircon standard R33 (age = 419 Ma; Black et al., 2004) and zircon trace

Table 1
Summary of samples and locations.

Sample name	Alt. Sample name[a]	Latitude[b]	Longitude[b]	Elevation (m)	Rock type	Description	Zircon?
bas1	ÖlE1301	N64°27.646′	W21°56.104′	105	Basalt	Ölver tholeiite	
gab1	HrI1202	N64°27.174′	W21°52.057′	388	Gabbro	Hrossatungar gabbro, slight alteration	✓
grn1	FlI1201	N64°29.988′	W21°55.057′	90	Granophyre	Flyðrur granophyre	✓
rhy1	SvE1302	N64°29.526′	W21°47.224′	541	Rhyolite	Svartitindur rhyolite; highly altered (QSP)	✓
rhy2	BrE1201	N64°31.321′	W21°47.377′	68	Rhyolite	Brekkufjall rhyolite, highly altered	✓
rhy3	TuE1301	N64°30.686′	W21°50.674′	628	Rhyolite	Tungukollur rhyolite	✓
rhy4	FeE1301	N64°35.244′	W21°45.383′	20	Rhyolite	Ferjubakki rhyolite, not in central volcano	✓
rhy5	ShE1302	N64°29.702′	W21°40.592′	377	Rhyolite	Skessuhorn rhyolite	✓
rhy6	RnE1201	N64°27.276′	W21°47.154′	556	Rhyolite	Rauðihnúkur rhyolite; moderate alteration	✓
rhy7	DrE1302	N64°30.987′	W21°34.726′	260	Rhyolite	Drageyraröxl ignimbrite; flow-banded and moderately altered	✓

[a] These names are reported in the Supplemental material.
[b] All coordinates are WGS84.

element concentrations were standardized relative to MADDER green zircon (3435 ppm U). Data were reduced using Squid 2.51 (Ludwig, 2009) and Isoplot 3.76 software (Ludwig, 2012). Measured $^{206}Pb/^{238}U$ were corrected for common Pb using ^{207}Pb based on a model Pb composition from Stacey and Kramers (1975) and corrected for ^{230}Th disequilibrium using the method of Schärer (1984) assuming an initial $(^{230}Th/^{238}U)_{melt}$ value based on whole rock Th/U values for each sample. The magnitude of the correction was typically 80 to 100 kyr.

After U-Pb and trace element analysis, zircon mounts were re-imaged via CL and the Lu—Hf isotope composition was measured on a subset of the same grains using LA-MC-ICPMS at the Radiogenic Isotope and Geochronology Laboratory at Washington State University. Fifty-eight total grains from 5 samples (rhy2, rhy3, rhy6, rhy7, and grn1) were analyzed for Lu—Hf isotope composition using a ThermoFinnigan Neptune MC-ICP-MS coupled to a New Wave 213 nm Nd-YAG laser with an analytical spot diameter of 40 μm, a 10 Hz repetition rate, and fluence of ~6 J/cm^3. We follow the instrument configuration, operating parameters, and data reduction methods outlined by Fisher et al. (2014), with the exception that U-Pb ages were not simultaneously determined. We used Mud Tank ($^{176}Hf/^{177}Hf = 0.282507 \pm 6$; Woodhead and Hergt, 2005) to normalize the mass-bias corrected $^{176}Hf/^{177}Hf$ for inter-laboratory comparison. Given the narrow range of Hf isotope composition present in Icelandic rocks, and the very large range of (Lu + Yb)/Hf present in H-S zircon samples combined with the importance of highly accurate correction for the isobaric interference of ^{176}Yb and ^{176}Lu on ^{176}Hf, secondary zircon standards used in this study covered the range of (Lu + Yb)/Hf of the samples studied. Analyses of secondary standards, determined by solution-MC-ICPMS, included GJ-1 ($^{176}Hf/^{177}Hf = 0.282000 \pm 23$; Morel et al., 2008) and MUNZirc4 ($^{176}Hf/^{177}Hf = 0.282135 \pm 7$; Fisher et al., 2011), and were interspersed with unknowns to assess accuracy and external reproducibility. LA-MC-ICPMS analyses of GJ-1 and MUNZirc4 yielded mean values for $^{176}Hf/^{177}Hf$ of 0.282002 ± 32 (2SD; $n = 15$) and 0.282131 ± 18 (2SD; $n = 13$; $^{176}Yb/^{176}Hf$ ~0.08 to 0.26), respectively. Analyses of these secondary zircon standards agree well with published solution-MC-ICPMS determination of the isotope composition of purified Hf from these zircons. Present day ε_{Hf} values were calculated using the CHUR parameters reported by Bouvier et al. (2008). Laser Lu—Hf isotopic data are reported with 2σ uncertainty in Table 3 and Supplemental Table S4. Analyses were not incorporated into the weighted mean sample age, $\delta^{18}O$, or ε_{Hf} values were omitted if they were outliers for being >2 standard deviations from the mean.

4. Results

4.1. Whole rock elemental compositions

Major and trace element compositions of the eight silicic and two mafic units sampled at H-S are listed in Table 2, together with whole rock Nd, Hf, and Pb isotope ratios.

Petrographic analysis (Supplemental Table S8) indicates all samples are altered to varying degrees, and therefore concentrations of some major and trace elements—such as Si, alkalis, Ca, and fluid-mobile trace elements—may not represent primary compositions. SiO_2 in rhyolites ranges from 69 to 80 wt%. The most strongly altered samples are rhy1 and rhy2. When compared to other silicic samples from this study, whole rock analyses reported by Franzson (1978), and compositions of unaltered rhyolites in general, it is evident that rhy2 is strongly enriched in Ca (secondary calcite is visible in thin section). Rhy1, which displays extensive quartz-sericite-pyrite alteration, has lost almost all Na and Ca and probably gained Si, consistent with strong hydrothermal alteration. Rare earth element (REE) concentrations, and especially the characteristics of chondrite-normalized REE patterns (Fig. 2), are unlikely to have been strongly affected by alteration. All silicic samples have high heavy REE (HREE), which is typical of Icelandic rhyolites (e.g. Jónasson, 2007). Samples rhy3–7 and grn1 are strongly enriched in light REE (LREE) relative to HREE, and with one exception (rhy3) have deep negative Eu anomalies; these characteristics are also typical of Icelandic rhyolites. Rhy 1 and rhy2 show only slight enrichment in LREE relative to HREE and pronounced relative depletion in middle REE (MREE), and their negative Eu anomalies are small. These characteristics are unlikely to be a consequence of alteration but are consistent with effects of accessory mineral (e.g. apatite, chevkinite, titanite) removal in residues of melting or crystallization.

The two mafic samples lack any obvious geochemical indicators of alteration. Basalt bas1 and gabbro gab1 have 50 and 44 wt% SiO_2, respectively. Bas1 has elemental chemistry generally similar to evolved basalts erupted from the currently propagating Eastern rift zone (Chauvel and Hémond, 2000; Sigmarsson et al., 2008). It is moderately enriched in LREE and lacks an Eu anomaly. Gabbro sample gab1 has a subparallel REE pattern but lower concentrations and a slight positive Eu anomaly that suggests plagioclase accumulation.

Zircon saturation temperatures were calculated from whole-rock analyses using both the original method of Watson and Harrison (1983; W&H) and the revised calibration of Boehnke et al. (2013; B) (Supplemental Table S5). Meaningful temperature estimates require that a sample represent a zircon-saturated magma and that the whole-rock composition approximates that of the melt. The calculated temperatures for the two mafic samples are unrealistically low (660 and 540 °C (W&H), 553 and 407 °C (B)). This is to be expected, because natural melts with mafic compositions are strongly undersaturated in zircon; zircon in mafic rocks like samples like gab 1 is either xenocrystic or grew at low T from trapped, fractionated melt. We disregard these two samples in further discussion of zircon saturation. Two other samples yield highly unrealistic temperatures: rhy1 and rhy2. As a consequence of extreme alteration, the compositions of these samples differ drastically from melts and their "M" values used in the saturation equation are far from the true value. The other samples all bear zircon (presumably zircon-saturated) and are phenocryst-poor (thus whole-rock composition is close to melt composition, if as appears to be the case, alteration is modest). Calculated temperatures using Watson and Harrison (1983) are systematically higher than those from Boehnke et al. (2013), but the difference at relatively high temperature is fairly small (Boehnke et al., 2013); for our samples, it ranges from 14 to 37 °C. Excluding the mafic and highly altered samples, our calculated temperatures range from 883 to 946 °C (W&H) or 846–932 °C (B). Less altered samples from the same units as rhy1 and rhy2, analyzed by Franzson (1978), yield similar temperatures of 892 and 857 °C (W&H) or 862 and 824 °C (B). The zircon saturation temperature range for H-S is typical of silicic volcanic whole rocks and glasses from Iceland (Carley et al., 2011; Claiborne et al., 2018).

4.2. Whole rock Nd, Hf, and Pb isotopes

Neodymium, hafnium, and lead isotopic ratios for five silicic and the basaltic (bas1) whole rock samples are within established ranges for Icelandic rocks (Figs. 3, 4; Table 2) (e.g. Peate et al., 2010; Willbold et al., 2009). The $^{143}Nd/^{144}Nd$ ratios of H-S rocks define a restricted range (0.513010–0.513030; ε_{Nd} + 7.2 to +7.6); silicic and mafic samples overlap within uncertainty. $^{176}Hf/^{177}Hf$ ratios range from 0.283109–0.283162 (ε_{Hf} + 11.4 to +13.3). H-S samples plot on or slightly below the Hf—Nd terrestrial array (Fig. 3), in a field overlapping that of the Icelandic Eastern Volcanic Zone (EVZ), a propagating rift environment (cf. Peate et al., 2010). Younger volcanic samples have somewhat lower ε_{Hf} than older samples (see discussion below). Most Icelandic lavas define a tight linear array below the Northern Hemisphere Reference Line (NHRL; Hart, 1984) on a $^{207}Pb/^{204}Pb$ vs. $^{206}Pb/^{204}Pb$ diagram and extend to both sides of the NHRL on a $^{208}Pb/^{204}Pb$ vs. $^{206}Pb/^{204}Pb$ diagram (Fig. 4). The H-S samples occupy a relatively restricted area in Pb—Pb space, with $^{206}Pb/^{204}Pb = 18.97$ to 19.11, $^{207}Pb/^{204}Pb = 15.51$ to 15.53, and $^{208}Pb/^{204}Pb = 38.52$–38.68 (Fig. 4). Lead ratios in sample grn1, the lone granophyre, are the least

Table 2
Whole rock analyses from Hafnarfjall-Skarðsheiði samples.

	Sample name and description									
	rhy1	rhy2	rhy3	rhy4	rhy5	rhy6	rhy7	grn1	gab1	bas1
	Rhyolite	Rhyolite	Rhyolite	Rhyolite	Rhyolite	Rhyolite	Rhyolite	Granophyre	Gabbro	Basalt
SiO_2	79.92	68.62	78.29	75.64	74.41	73.63	74.73	73.33	43.31	50.36
TiO_2	0.24	0.18	0.20	0.16	0.20	0.31	0.27	0.38	3.92	1.97
Al_2O_3	12.77	12.21	11.67	11.99	12.75	13.00	12.37	12.52	12.16	15.51
FeO(total)	2.64	1.52	2.21	2.73	3.04	3.25	2.74	4.37	18.00	10.68
MnO	0.00	0.23	0.02	0.06	0.03	0.10	0.05	0.15	0.24	0.19
MgO	0.21	0.21	0.09	0.07	0.10	0.05	0.21	0.17	6.88	6.30
CaO	0.05	8.91	0.25	1.09	0.42	1.41	0.28	1.51	12.35	11.57
Na_2O	0.10	4.29	4.29	5.05	4.83	4.70	4.56	4.97	2.04	2.53
K_2O	3.34	3.18	2.49	3.14	3.24	2.29	3.54	2.66	0.16	0.56
P_2O_5	0.01	0.02	0.02	0.01	0.03	0.02	0.03	0.05	0.08	0.26
Sum	99.28	99.36	99.55	99.94	99.05	98.77	98.79	100.09	99.13	99.93
LOI	3.71	7.36	1.35	0.19	0.97	4.45	1.09	0.43	0.28	2.03
Sc	1.4	3.4	0.7	3.9	0.8	2.2	1.7	6.5	53.8	37.8
V	1	2	14	0	12	3	21	4	906	275
Cr	2	3	3	3	2	2	3	0.50	15	100
Ni	0	2	1	1	2	2	3	1	68	62
Cu	5	8	21	3	5	3	6	5	372	105
Zn	135	159	103	68	161	177	206	167	139	95
Ga	30	21	26	25	33	29	30	26	22	18
Rb	76	68	46	63	67	67	72	52	2	6
Sr	11	71	75	66	73	131	64	101	225	304
Y	74	78	73	114	78	123	90	131	18	33
Zr	595	415	452	510	507	765	585	850	79	186
Nb	114	76	93	96	120	99	133	91	10	22
Cs	0.5	0.4	0.1	0.2	0.1	1.0	0.3	0.1	0.0	0.0
Ba	409	489	529	528	650	663	636	521	42	132
La	26.0	27.1	169.7	71.7	114.4	83.7	90.2	80.5	5.7	18.4
Ce	42.8	57.5	263.2	158.1	205.1	180.2	170.0	177.2	14.1	41.7
Pr	5.6	9.0	40.0	19.9	29.3	22.8	23.0	23.0	2.2	5.7
Nd	21.2	35.7	140.2	79.2	115.2	91.0	89.1	94.8	10.5	25.0
Sm	5.9	8.9	32.0	19.0	24.9	21.6	19.5	22.5	3.2	6.3
Eu	1.7	2.3	8.2	2.9	4.6	4.4	3.6	4.7	1.3	2.0
Gd	7.8	8.6	27.8	18.7	21.8	21.4	17.7	22.6	3.7	6.6
Tb	1.8	1.8	4.4	3.4	3.6	3.8	3.1	4.0	0.7	1.1
Dy	13.7	12.7	21.7	21.7	20.7	23.8	18.9	25.4	3.9	6.7
Ho	3.2	2.9	3.5	4.5	3.8	4.9	3.8	5.2	0.8	1.3
Er	10.0	8.8	8.4	12.6	9.7	13.4	10.1	14.5	2.0	3.6
Tm	1.7	1.5	1.2	1.9	1.4	2.0	1.5	2.1	0.3	0.5
Yb	11.0	9.4	6.8	12.2	8.5	11.9	9.1	12.9	1.6	3.0
Lu	1.7	1.5	1.0	1.9	1.2	1.8	1.3	2.0	0.2	0.5
Hf	18.8	12.6	14.9	15.9	17.8	20.5	18.4	22.0	2.3	4.8
Ta	7.7	5.4	6.7	6.7	8.5	6.5	8.7	5.8	0.7	1.5
Pb	8.8	6.2	7.9	3.3	7.4	7.0	8.0	5.0	0.6	1.6
Th	12.9	10.8	9.6	12.0	11.6	9.4	12.6	8.9	0.5	1.8
U	3.3	2.2	2.7	3.1	2.5	2.8	3.6	2.6	0.1	0.5
$^{143}Nd/^{144}Nd$[a]	–	0.513015 (12)	0.513010 (10)	–	–	0.513010 (8)	0.513012 (9)	0.513030 (9)	–	0.513028 (11)
εNd	–	+7.4	+7.2	–	–	+7.2	+7.3	+7.6	–	+7.6
$^{176}Hf/^{177}Hf$[a]	–	0.283161 (7)	0.283148 (7)	–	–	0.283120 (6)	0.283108 (5)	0.283136 (6)	–	0.28
εHf	–	+13.3	+12.8	–	–	+11.9	+11.5	+12.4	–	+11.9
$^{206}Pb/^{204}Pb$[a]	–	18.9724 (12)	19.0369 (20)	–	–	18.9680 (12)	19.1136 (12)	18.9466 (19)	–	19.0402 (20)
$^{207}Pb/^{204}Pb$[a]	–	15.5238 (10)	15.5271 (20)	–	–	15.5140 (9)	15.5232 (10)	15.5134 (20)	–	15.5244 (20)
$^{208}Pb/^{204}Pb$[a]	–	38.5641 (23)	38.6236 (55)	–	–	38.5462 (24)	38.6783 (23)	38.5207 (55)	–	38.6081 (56)
Zircon Sat (°C)[b]	892[d]	857[d]	909	881	902	946	921	939	536	663
Zircon Sat (°C)[c]	862[d]	824[d]	636	608	629	673	648	915	407	553

[a] Reported errors are in-run 2SE.
[b] Calculated using the method of Watson and Harrison (1983) assuming that whole rock compositions of these phenocryst-poor rocks approximate melt composition.
[c] Calculated using the method of Boehnke et al. (2013) assuming that whole rock compositions of these phenocryst-poor rocks approximate melt composition.
[d] For visibly altered samples rhy1 and rhy2, data from equivalent samples from Franson, 1978 were substituted. Full calculation in the Supplemental Material.

radiogenic of the H-S samples. Pb-isotope ratios generally follow those measured from the propagating EVZ (Peate et al., 2010) (Fig. 4). No whole rock radiogenic isotope ratios correlate with major element composition.

4.3. Zircon U-Pb geochronology

Zircon U-Pb ages from sampled silicic units at Hafnarfjall-Skarðsheiði indicate two distinct crystallization phases: an earlier Phase 1 and a later Phase 2. Individual spot analyses from Phase 1 rhyolite samples rhy1 ($n = 15$), rhy2 ($n = 43$), rhy3 ($n = 10$), and rhy4 ($n = 10$) yield ages that range from 4.93 ± 0.25 Ma to 5.86 ± 0.45 Ma (1σ SD), and Phase 2 rhyolite samples rhy5 ($n = 10$), rhy6 ($n = 10$), rhy7 ($n = 10$), granophyre grn1 ($n = 10$) and gabbro gab1 ($n = 16$) yield ages that range from 3.57 ± 0.14 Ma to 4.57 ± 0.10 Ma. Weighted mean ages for each sample are presented in Table 3 and full analytical results are in Supplemental Table S2. Weighted mean sample ages for Phase 1 range from 5.33 ± 0.04 Ma to 5.43 ± 0.14 Ma (2σ SE for weighted mean ages) and Phase 2 mean sample ages range from 3.90 ± 0.20 Ma to 4.38 ± 0.11 Ma (Fig. 5a). One grain from rhyolite rhy2 yielded a much older age of 11.34 ± 0.17 Ma (1σ SE), thus documenting inheritance. The range of values for mean squared weighted deviations

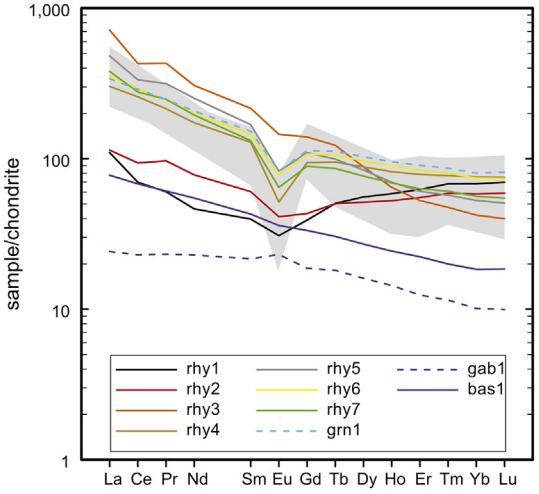

Fig. 2. H-S whole rock REE normalized to chondrite values (McDonough and Sun, 1995). Intrusive samples denoted by dashed lines. Typical compositions of Icelandic rhyolites denoted by grey field (Jónasson, 2007).

(MSWD; weighted by $1/\sigma^2$) for calculated weighted mean ages is 0.42–3.1; several values above 1.5–2 suggest that at least some of the measured intrasample age variation is real (Mahon, 1996). Common Pb contamination ranges from near zero (samples rhy5, rhy3, and rhy7) to 65% in sample gab1, probably from inclusions.

4.4. Zircon trace elements

4.4.1. Ti and Hf

Titanium concentrations in H-S zircon range from 5 to 38 ppm (excluding outliers that we interpret to indicate the presence of inclusions; Fig. 6a, Supplemental Table S3). Hafnium concentrations range from ~6800 ppm to 12,300 ppm (mean ~9500 ppm) (Fig. 6a, b). Zircons from the intrusive units (gab1 and grn1) are higher in Ti and somewhat lower in Hf than those from the extrusive units, averaging ~8000 ppm Hf at ~19 ppm Ti (gab1) and ~9000 ppm Hf at ~22 ppm Ti (grn1). Several of the volcanic samples—especially rhy5 and rhy1—show a wide range of intra-sample variability. Samples rhy2 and Rhy7 have the most restricted range of Ti and Hf. Despite these variations, the majority of volcanic H-S data form a coherent population within the greater Iceland zircon compositional array (Fig. 6) (Carley et al., 2014). Ti concentrations are not correlated with age.

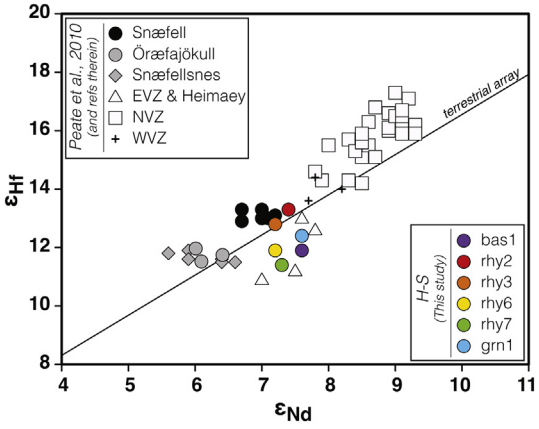

Fig. 3. Whole rock ε_{Hf} vs. ε_{Nd} data from H-S plotted against the Iceland array of Peate et al. (2010). Note the similarity to the sparse Heimaey/EVZ (propagating rift) samples. Öræfajökull, Snæfell, and Snæfellsnes are off-rift; NVZ and WVZ are on-rift. Terrestrial array ($\varepsilon_{Hf} = 1.36\varepsilon_{Nd} + 2.95$) after Vervoort et al. (1999). Modified from Peate et al. (2010) and references therein.

We applied the Ti-in-zircon thermometer of Ferry and Watson (2007) to our measured zircon Ti values. In addition to reliable Ti concentrations, reasonable estimates of a_{TiO2} and a_{SiO2} are critical for application of this thermometer. Titanium is invariably very low in zircon crystals, and therefore minute inclusions of other minerals or melt included within the analytical volume result in erroneous high measured values. Based on unusually high concentrations of elements that are much lower in zircon than in potential included phases (e.g. Fe, Al, Na, K) as well as high Ti, we reject all of the analyses with Ti > 40 ppm. Ferry and Watson (2007) and Watson et al. (2006) note a common a_{TiO2} range of 0.6 to 0.9 in silicic magmas; Ghiorso and Gualda (2013) suggest a wider a_{TiO2} range, from 0.3 to 0.9. The a_{SiO2} of silicic (rhyolitic) magmas is generally assumed to have a much narrower range, approaching or equal to unity (quartz saturation). We bracketed a_{TiO2} and a_{SiO2} (0.3–0.8 and 0.7–1.0, respectively) to constrain the possible temperatures reflected by Ti concentrations. Excluding the suspect high-Ti outliers and a single very low Ti concentration, our four modeled activity scenarios yielded ranges of Ti-in-zircon temperatures of 690–920, 700–930, 730–980, and 780–1060 °C for the 157 measured Ti concentrations (Supplemental Table S10). These ranges are consistent with those determined for zircon data from throughout Iceland (Carley et al., 2011, 2014, 2017). The results strongly support a wide range of zircon crystallization temperatures, with the lower portion near the low-pressure solidus and far lower than calculated H-S zircon saturation temperatures. The upper ends of three of the four simulations are similar to the higher saturation temperatures; the fourth is considerably higher.

4.4.2. Rare Earth elements (REE)

Chondrite-normalized zircon REE patterns are shown in Fig. 6c and Supplemental Table S3. Several samples (rhy1, rhy2, and gab1) have patterns that are relatively enriched in light REE (LREE), probably due to the presence of small inclusions (either minerals or melt), which are common in zircon (e.g. Claiborne et al., 2018). Ubiquitous positive Ce and negative Eu anomalies in chondrite-normalized plots (Supplement) are consistent with trends observed in all other silicic Icelandic zircons, and in zircon generally (e.g. Carley et al., 2011; Hoskin and Schaltegger, 2003). HREE are greatly enriched relative to chondrite and span more than an order of magnitude, from ~1000 to >10,000× chondrite. HREE/MREE concentrations rise subtly but distinctly as REE concentrations increase (Fig. 6c), with older samples having slightly higer Yb/Sm than younger ones. Sample rhy5 has higher concentrations and smaller intergrain variation in REE concentration than other H-S samples, which suggests growth from a uniform and strongly fractionated melt.

4.5. In situ zircon O isotopes

Oxygen isotope ratios ($\delta^{18}O$) for zircon from eight silicic samples are low compared to that estimated for zircon equilibrated with mantle-derived magma (~5.3‰; Valley, 2003), ranging from 1.5 to 4.6‰ with a mean value for all analyses of 2.8‰ (Table 3; Fig. 5b; Supplemental Table S1). Sample rhy6 has the highest weighted mean value ($\delta^{18}O = 3.4 \pm 0.2$‰; 2SE), and sample rhy2 has the lowest ($\delta^{18}O = 2.2 \pm 0.1$‰). Granophyre grn1 displays the widest range of values, from ($\delta^{18}O$~0.6 to 4.6‰). MSWDs vary from 2.9 (rhy7) to 167 (rhy5), demonstrating modest to large intrasample variability.

4.6. In situ zircon Hf isotopes

Hafnium isotope compositions were obtained for zircons from five H-S samples. The range of ε_{Hf} for the H-S zircon population ($n = 62$) is +8.3 to +13.2 (Table 3; Fig. 5c; Supplemental Table S4). Samples rhy2 and rhy3, which have nearly identical U-Pb ages, have average ε_{Hf} of +11.7 ± 0.8 (2SE; MSWD = 2.4) and + 11.5 ± 0.4 (MSWD = 1.4), respectively. Average values for samples rhy6 ($\varepsilon_{Hf} = +10.8 \pm 1.2$; MSWD = 4.7), rhy7 ($\varepsilon_{Hf} = +11.2 \pm 0.3$; MSWD = 1.2), and grn1

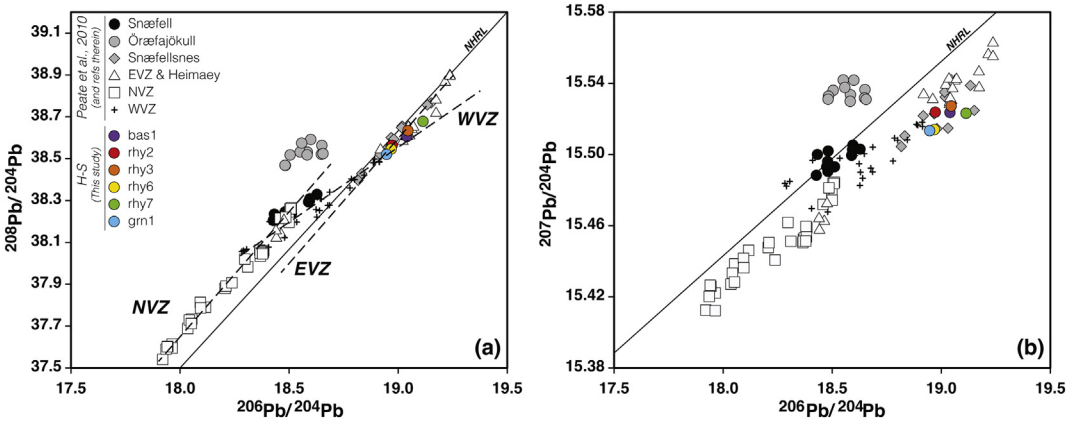

Fig. 4. Whole rock Pb isotope compositions of H-S samples and basalts from several Icelandic volcanic regions. a) $^{208}Pb/^{204}Pb$ vs. $^{206}Pb/^{204}Pb$ for Icelandic volcanic regions. H-S plots in an overlapping space with modern Heimaey/EVZ and Snæfellsnes. The NVZ and WVZ are established rifts while the EVZ is a propagating rift. b) Whole rock $^{207}Pb/^{204}Pb$ vs. $^{206}Pb/^{204}Pb$ for modern Iceland rift zones. H-S samples clearly overlap with those from the EVZ. Modified from Peate et al. (2010) and references therein. Trend lines estimated by Peate et al. (2010).

($\varepsilon_{Hf} = +11.7 \pm 0.6$; MSWD = 2.5) are also statistically indistinguishable at the 2σ level. Zircons from samples rhy3 (ε_{Hf} from +10.3 to +12.6) and rhy7 (ε_{Hf} from +10.1 to +12.1), have the most restricted intra-sample ε_{Hf} ranges of ~2 epsilon units, while zircon ε_{Hf} from samples rhy 2 (ε_{Hf} from +9.1 to +13.7), rhy6 (ε_{Hf} from +8.3 to +12.7), and grn1 (ε_{Hf} from +9.6 to +13.2) have larger ranges (up to 4.6 epsilon units) of ε_{Hf}. Overall, H-S zircon ε_{Hf} values are within the range of typical Icelandic zircon values (Carley et al., 2017; Padilla et al., 2016).

5. Discussion

5.1. Timing and duration of silicic magmatism

U-Pb zircon crystallization ages from all eight silicic units (rhyolites rhy1–7; granophyre grn1) record two distinct phases of silicic crystallization: Phase 1 at 5.43 ± 0.13 Ma to 5.32 ± 0.18 Ma (2SE for weighted mean ages) and Phase 2 from 4.38 ± 0.11 Ma to 4.13 ± 0.11 Ma, with the granophyre grn1 representing the youngest age at 3.90 ± 0.20 Ma. Zircon from gabbro gab1 has an age of 4.00 ± 0.08 Ma; we infer that these grains crystallized from fractionated silicic melt. Zircon crystallization in the granophyre unit occurred roughly 200 kyr after that of zircon from any of the other silicic units. Based on our analyses, duration of Phase 2 volcanic zircon crystallization was ~2 times longer than Phase 1 zircon crystallization, which may imply a shift in petrogenetic processes and/or magma sources over time. The U-Pb zircon ages from silicic units presented here deviate from those inferred based on paleomagnetic constraints and K-Ar ages (Franzson, 1978) and references therein (cf. Supplemental Table S6). All samples show a range of at least a few hundred kyr in zircon crystallization ages. Some of this variability is attributable to analytical precision, but MSWDs for some samples that reach 2–3 suggest that our zircon populations do document a growth over an extended time period. This phenomenon has been described in other locations, where it is interpreted to indicate long-term storage in near- to sub-solidus conditions and/or entrainment of antecrysts in ascending magma (e.g. Claiborne et al., 2010; Schmitt et al., 2010; Barboni et al., 2016; and many others). Timescales of residence indicated by our data appear to be much greater than previously suggested for young (<~50 kyr) Icelandic volcanic systems (Carley et al., 2011).

Silicic magmatism at H-S lasted for at least 1.5 Myr—one of the longest known durations of silicic volcanism at any central volcano in Iceland (cf. Carley et al., 2017). The overall lifespans of central volcanoes are commonly considered to be 300 kyr to ~1 Myr (Sæmundsson, 1986). If paleomagnetic age estimates of the basalts that precede and follow the silicic units at H-S are accepted (Franzson, 1978), the overall lifespan of Hafnarfjall-Skarðsheiði central volcano is at least 2 Myr.

Hafnarfjall-Skarðsheiði central volcano unconformably overlies Mio-Pliocene bedrock erupted from the SSRZ despite being composed of younger Pliocene material erupted from the WRZ. In contrast, most other areas with significant silicic magmatism and Mio-Pliocene bedrock in western Iceland erupted from the SSRZ. H-S is therefore uniquely situated to record the processes and timescales associated with silicic magma genesis post-dating rift relocation. During rift relocation, both the declining and incipient rifts receive magma (e.g. Benediktsdóttir et al., 2012; Harðarson et al., 2008; Martin and Sigmarsson, 2010). Establishing the duration of the interval between rift relocation and initial silicic magma production requires constraining the time at which oldest silicic rocks were formed. Martin and Sigmarsson (2010) suggest that SSRZ magmatism transitioned to the WRZ sometime between 6.7 and 5.5 Ma, indicating that the hiatus between onset of rift-related basaltic magmatism and the initiation of silicic magmatism was between ~0 and 1.3 Myr, based on the zircon crystallization sample age of rhy1.

Table 3
In situ zircon analysis summary: weighted sample means and statistics.

	U-Pb geochronology				Oxygen isotopes				Hafnium isotopes			
	Age (Ma)	2 SE[a]	*n* of N	MSWD	$\delta^{18}O$ (‰)	2 SE[a]	*n* of N	MSWD	εHf	2 SE[a]	*n* of N	MSWD
rhy1	5.43	0.13	15 of 15	1.7	2.8	0.3	7 of 8	13	–	–	–	–
rhy2	5.33	0.04	43 of 45	1.07	2.2	0.1	26 of 27	11.1	+11.7	0.8	11 of 11	2.4
rhy3	5.32	0.10	10 of 10	0.42	2.9	0.2	23 of 24	13	+11.5	0.4	14 of 14	1.4
rhy4	5.32	0.18	10 of 12	2.2	2.5	0.3	8 of 8	29	–	–	–	–
rhy5	4.38	0.11	10 of 10	2.0	2.8	1.0	5 of 7	167	–	–	–	–
rhy6	4.22	0.25	10 of 10	3.1	3.4	0.2	24 of 24	12	+10.8	1.2	9 of 9	4.7
rhy7	4.13	0.11	10 of 10	1.5	3.2	0.1	28 of 30	2.9	+11.2	0.3	15 of 15	1.2
gab1	4.00	0.08	16 of 16	1.19	–	–	–	–	–	–	–	–
grn1	3.90	0.20	10 of 10	1.7	2.7	0.3	27 of 28	58	+11.7	0.6	13 of 13	2.5

[a] Standard error of each sample, not including internal and external uncertainties.

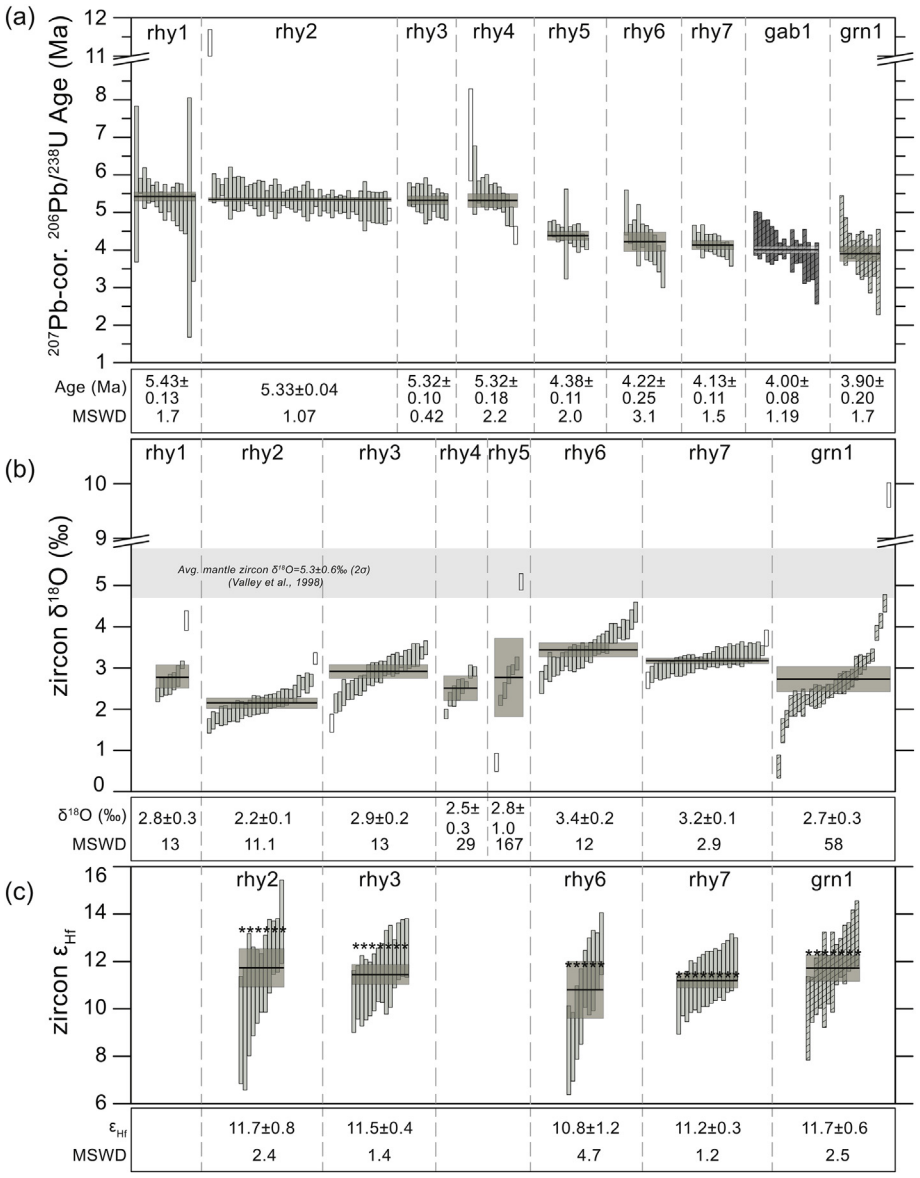

Fig. 5. Zircon analyses from H-S samples. Each vertical bar is a single analysis+2SE; open vertical bars are analyses that Isoplot rejected from the population; patterned boxes denote intrusive samples; darker shading denotes mafic composition; horizontal boxes denote weighted sample means+2SE; thick black horizontal lines denote weighted sample means. Weighted sample means+2SE listed for each sample. (a) U-Pb ages. Ages are also corrected for ^{230}Th disequilibrium. (b) Oxygen isotope compositions. Average mantle zircon value from Valley et al. (1998) shown by large horizontal grey field. (c) ε_{Hf} values. Horizontal stars are approximate corresponding whole-rock ε_{Hf} values.

5.2. Implications of isotopic data

5.2.1. Overview of Iceland oxygen isotope variation

Zircon crystallizing from melt generated through closed-system fractionation of mantle-derived magma is suggested to have $\delta^{18}O = 5.3 \pm 0.6‰$ (Valley, 2003; Valley et al., 1998; Valley et al., 2005). Crystallization leads to an increase in $\delta^{18}O$ in fractionated melt, and therefore values lower than ~5.3‰ indicate that zircon crystallized from magmas with a substantial component of unusually low-^{18}O material; $\delta^{18}O$ in H-S zircon is well below this value.

In Iceland, two mechanisms for abundant production of Icelandic magmas with $\delta^{18}O$ lower than expected mantle values have been proposed: (1) Many basaltic magmas and most silicic magmas in Iceland contain a hydrothermally altered crustal component, or (2) the Icelandic mantle contains a major component that has lower $\delta^{18}O$ than typical mantle. Mechanism (1) is more conventional, having been applied to low-$\delta^{18}O$ silicic rocks and constituent minerals worldwide (e.g. Bindeman, 2008): depletion in ^{18}O relative to ^{16}O in magmas (and zircons that crystallize from them) is interpreted to indicate source material (or a major assimilant) that underwent high temperature alteration by meteoric or sea water. Mechanism (2) has been suggested because many Icelandic basalts have $\delta^{18}O$ lower than typical mantle (~5.3‰). Thirlwall et al. (2006) suggest that the Icelandic mantle has $\delta^{18}O$ values that range downward toward ~4‰. More recent examination of olivine crystal cargos in Icelandic basalts suggests that low-^{18}O magmas result from hydrothermal alteration by isotopically light meteoric water, or through anatexis or assimilation of such material (Bindeman et al., 2012, 2008; Gurenko and Chaussidon, 2002).

It is well established that the dominantly basaltic Icelandic crust has low $\delta^{18}O$, commonly ranging from ~2 to 6‰ at the surface and from −10.5 to 6‰ at depth (e.g. Muehlenbachs et al., 1974; Hattori and Muehlenbachs, 1982; and many others), and most basalts erupted in the last ~0.7 Myr have $\delta^{18}O$ ranging from ~3.5‰ to 5.5‰ (Pope et al., 2013 and sources therein). Pope et al. (2013) present a model for basalts at the modern Krafla volcano in which a mantle-derived basalt ($\delta^{18}O = 5.5‰$) repeatedly assimilates ~15% melt from hydrothermally altered

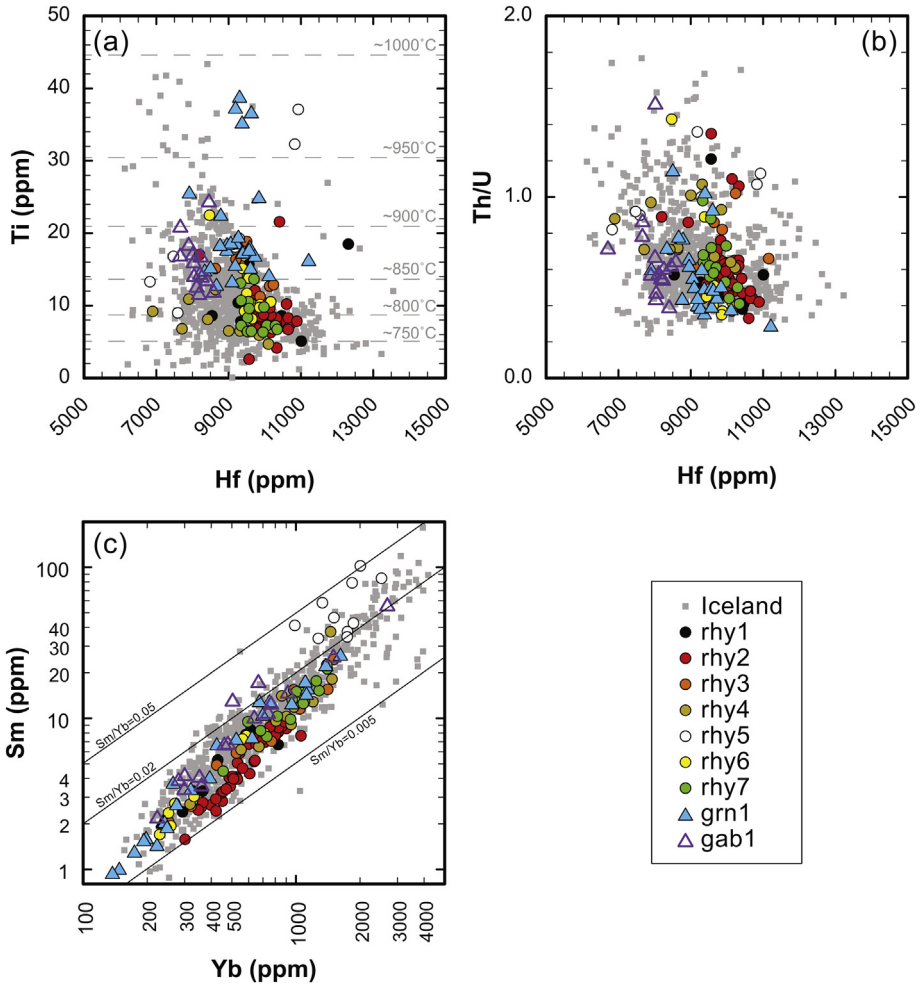

Fig. 6. Trace elements in H-S zircon plotted against the Iceland zircon array from Carley et al. (2014). (a) Ti vs. Hf concentrations. Zircon crystallization temperatures calculated using the method of Ferry and Watson (2007) with $a_{SiO2} = 1.0$ and $a_{TiO2} = 0.5$. (b) Th/U vs. Hf. (c) Sm vs. Yb. Lines of constant Sm/Yb shown for reference.

bedrock ($\delta^{18}O = -10‰$) to produce a magma with final $\delta^{18}O = 4.7‰$ over 15 Myr, but it should be noted that altered crust with $\delta^{18}O$ as low as −10‰ is unusual for Iceland as a whole (Hattori and Muehlenbachs, 1982).

5.2.2. Implications of oxygen isotopic compositions of Hafnarfjall-Skarðsheiði zircon

Zircons from H-S silicic units have $\delta^{18}O$ ranging from ~1.6 to 4.4‰, with sample means between 2.2 and 3.4‰. These values are within the typical range of $\delta^{18}O$ for Icelandic zircons; 90% of Icelandic zircons have $\delta^{18}O$ ranging from 0.2‰ to 4.7‰ (mean $\delta^{18}O$ of 3.0‰) (Carley et al., 2014). $\delta^{18}O$ in zircon is substantially lower than the $\delta^{18}O$ in melt from which it grows—for rhyolitic melt, the difference is roughly 1.8‰ at 850 °C (Bindeman et al., 2012; Trail et al., 2009). Melt also has higher $\delta^{18}O$ than the bulk crystallizing assemblage; current estimates are that extended closed-system crystallization of mafic magma melt leads to an increase of roughly 0.5 to 1‰ in $\delta^{18}O$ in fractionated rhyolite melt (e.g. Bindeman, 2008; Trail et al., 2009; cf. Valley et al., 2005). A comparably higher $\delta^{18}O$ in anatectic melt than in altered basalt source is anticipated. $\delta^{18}O$ in zircon is expected to remain nearly constant as a consequence of closed-system processes (Valley et al., 2005) and be near 5.3‰ for zircon in silicic magmas derived by fractional crystallization of "normal" mantle-derived basalt.

Results of mass balance modeling aimed at constraining relative contributions of materials potentially required to produce the H-S average zircon $\delta^{18}O$ (~2.8‰) are outlined below (with full details in Supplemental Table S7) (cf. Pope et al., 2013). Interpretation based on such modeling is complicated by plausible variability in altered crust ($-2 > \delta^{18}O > -10‰$; Hattori and Muehlenbachs, 1982) and in mantle basalt (~4 to 5.5‰; e.g. Pope et al., 2013). For example, zircon crystallizing from a melt composed of a 3:2 ratio of rhyolite melt derived from fractional crystallization of mantle basalt ($\delta^{18}O$ ~5.5‰) and rhyolite melt derived from anatexis of crust with $\delta^{18}O$~2‰ will have $\delta^{18}O$ ~2.8‰—as will zircon crystallizing from a 9:1 ratio of rhyolite melt derived from fractional crystallization of mantle basalt ($\delta^{18}O$~5.5‰) and rhyolite melt derived from anatexis of crust with $\delta^{18}O = -10‰$ (Supplemental Table S7). Despite the uncertainty regarding input compositions, two conclusions on H-S rhyolite petrogenesis may be drawn from these models: (1) melt produced by fractional crystallization of mantle-derived magma appears likely to have been the dominant component; however, (2) a substantial fraction of anatectic melt (or bulk assimilation) of low-$\delta^{18}O$ crust is required to generate the observed zircon $\delta^{18}O$ values. Large intrasample variability in zircon $\delta^{18}O$ (1–4 units; MSWD 3–67) demonstrates open-system behavior; zircons in individual samples must have gathered from multiple environments prior to final assembly of the erupted magma.

5.2.3. Implications of Nd-Hf-Pb isotopic compositions

The upper mantle beneath Iceland is isotopically heterogeneous and has been interpreted to be composed of at least 3–4 compositional end members: (1) a depleted mantle MORB-like source with unradiogenic Pb and Sr and high ε_{Nd} and ε_{Hf} (Kitagawa et al., 2008; cf. Hanan and Schilling, 1997, Thirlwall et al., 2004); (2) a primitive He-enriched source (e.g. Hilton et al., 1999) which may or may not be similar to

FOZO (Hanan and Graham, 1996; Hart et al., 1992); and incompatible element-enriched mantle with some combination of (3) EM-1 (relatively unradiogenic $^{206}Pb/^{204}Pb$, ε_{Nd}, and ε_{Hf}; moderate (~0.705) $^{87}Sr/^{86}Sr$ (e.g. Hanan and Schilling, 1997; Sigmarsson et al., 1992b; Thirlwall et al., 2004)) and (4) EM-2 (moderately radiogenic $^{206}Pb/^{204}Pb$, high $^{87}Sr/^{86}Sr$, low ε_{Nd}, and high ε_{Hf} (Kokfelt et al., 2006; Prestvik et al., 2001; Zindler and Hart, 1986)). Characteristics of the EM-2 component have been ascribed to incorporation of pelagic sediments or input from recycled oceanic crust (e.g. Hemond et al., 1993; Mertz and Haase, 1997; Peate et al., 2010; Sigmarsson and Steinthórsson, 2007; Thirlwall et al., 2004; Torsvik et al., 2015). It should be noted that evaluation of the origin of any of these end-member components, their precise compositions, or the precise composition of the Icelandic mantle is not the aim of this study. Furman et al. (1995) suggest that the scale of mantle heterogeneity is relatively small (10s of km), while Peate et al. (2010) suggest a NE-SW variation in the mantle source composition across Iceland that results in the NVZ and EVZ having parallel but offset trends in $^{207}Pb/^{204}Pb$ vs. $^{206}Pb/^{204}Pb$ plots and the EVZ and WVZ intersecting at a common source that is not involved in producing NVZ magmas (Fig. 3). Other researchers (e.g. Shorttle et al., 2013) show that Pb isotope compositions in Iceland are strongly dependent on geographic location and that Pb isotopes are decoupled from Nd (and presumably Hf) isotopes on length scales >140 km. Notably for H-S, Kitagawa et al. (2008) suggest that temporal variations in Tertiary lava Sr-Nd-Hf-Pb isotope geochemistry can be attributed to changes in the relative contributions of the various end-member components to the erupted magmas and correlated with temporal variations in magma productivity.

Lead isotopic data from H-S are quite uniform compared to Iceland as a whole and coincide with a portion of the array defined by EVZ basalt from the currently propagating Eastern rift zone (Fig. 4). Whole rock Nd and Hf isotope ratios are relatively uniform and unradiogenic compared to the bulk of Icelandic rocks (Fig. 3); as with Pb, Hf and Nd isotope data cluster fairly tightly and fall within the range of EVZ rocks but are distinct from those of the WVZ and NVZ. There is no clear distinction between the silicic and mafic samples, as is common in Iceland (e.g. Prestvik et al., 2001; Sigmarsson et al., 1991).

Based on the criterion of Martin and Sigmarsson (2010), H-S whole rock $^{143}Nd/^{144}Nd$ ratios (≥0.51297) suggest an on-rift petrogenetic environment. These authors propose that on-rift silicic magmas are generated dominantly through crustal anatexis and off-rift silicic magmas result from fractional crystallization. However, H-S samples occupy a relatively low Nd and Hf isotopic niche that clearly differs from basalts erupted from the NVZ and WVZ (Peate et al., 2010) (Fig. 3). Questions thus arise regarding petrogenesis of Icelandic magmas: (1) Would anatectic rhyolites have different Hf and Nd isotopic compositions than rhyolites produced by fractional crystallization of newly derived basalt? (2) Why should mantle melts produced at an establishing rift differ from those produced when a rift is fully formed? Anatectic rhyolites certainly could have different isotopic characteristics than those from fractional crystallization, but they also could have identical isotopic compositions (with the exception of oxygen) if the new, mantle-derived basalt has the same isotopic signature as the extant crust—a phenomenon observed elsewhere in Iceland (e.g. Krafla; Nicholson et al., 1991). The inference that 'on-rift' Nd (and, by implication, Hf) isotope compositions suggest anatexis at hot, high-flux rifts is potentially misleading, since the source of the anatectic melt is older underlying crust and thus radiogenic isotope ratios may be independent of extant tectonomagmatic setting.

As for question 2 above, there is good evidence that propagating systems produce mafic and silicic magmas with isotopic ratios that are transitional between those observed in established 'on-rift' settings and those from known 'off-rift' zones such as the Snæfellsnes and the Öræfajökull Volcanic Belts (e.g. Óskarsson et al., 1982; Hemond et al., 1993; Mertz and Haase, 1997; Martin and Sigmarsson, 2010; Peate et al., 2010; and many others). For example, Martin and Sigmarsson (2007) report silicic samples from Torfajökull in the EVZ have $^{143}Nd/^{144}Nd$ ratios of 0.51297 to 0.51298—barely within the 'on rift' field (boundary at $^{143}Nd/^{144}Nd$ ~0.51296-0.51297) of Martin and Sigmarsson (2010). Another study of Torfajökull rocks yielded $^{143}Nd/^{144}Nd$ ratios of 0.51296 to 0.51299 for bulk rock compositions from basalt through rhyolite, with no significant differences in isotopic compositions between the different rock types (Stecher et al., 1999). The transitional isotopic ratios produced in modern EVZ and H-S magmas could result from differences in influence of the plume component in petrogenesis during rift establishment. While isotopically heterogeneous, the putative plume component has generally higher $^{208}Pb/^{204}Pb$, $^{207}Pb/^{204}Pb$, and $^{206}Pb/^{204}Pb$, and less radiogenic Hf and Nd isotopes than the MORB component that dominates in a fully established rift (e.g. Hemond et al., 1993; Mertz and Haase, 1997; Peate et al., 2010). The plume initially appears to play a larger role in petrogenesis at a propagating rift while the MORB-source depleted mantle plays a subordinate role, with the roles gradually reversing as the rift becomes more established and fully matures. Rift relocation and establishment are tied to the location of the Iceland plume (Hardarson et al., 1997; Martin et al., 2011; Óskarsson et al., 1985)—once a rift segment drifts far enough from the plume to be relatively free of its thermal and magmatic influence, a new rift starts propagating at or close to the plume axis. A natural consequence of rift relocation is then not only variation in plume component vs. MORB component magma during evolution of the rift, but also variation in radiogenic isotope compositions of basaltic crust forming at the rift (and any magmas subsequently derived from it). Therefore, the Icelandic crust itself likely preserves isotopic heterogeneity imposed by >16 Myr of rift-plume interaction. If crustal isotopic heterogeneity is a consequence of rifting, areas that were at one time near a propagating rift axis are likely to have rocks with higher $^{208}Pb/^{204}Pb$, $^{207}Pb/^{204}Pb$, and $^{206}Pb/^{204}Pb$, and lower, less radiogenic Hf and Nd isotope ratios, as would any melt derived from those rocks. If anatexis occurs in areas where the crust formed at an established rift with the MORB-dominant component, then resulting silicic magmas will have Hf and Nd isotope ratios higher than in areas with a greater proportion of plume-derived magmas; fractional crystallization of a juvenile magma from an established rift would also yield those same higher Hf and Nd isotope compositions in the resulting silicic products. Therefore, the evolutionary state of the rift, crustal history, and mantle heterogeneity may all be important contributing factors to the isotopic composition of silicic Icelandic magmas, and isotopic compositional variation cannot solely be a result of an 'on rift' or 'off rift' location (cf. Martin and Sigmarsson, 2010; Óskarsson et al., 1985). Nd, Hf, and Pb isotopic compositions indistinguishable between mafic and silicic samples at H-S might reflect a juvenile, mantle-derived magma undergoing fractional crystallization to produce silicic magmas (although the O isotope data preclude this as the only mechanism by which silicic magmas could be produced) but could equally reflect anatexis of pre-existing crust with the observed isotopic compositions.

Whole rock Nd and Hf isotope compositions of H-S are relatively unradiogenic compared to the bulk of Icelandic rocks and are compositionally similar to modern EVZ products (Fig. 2). Statistically significant variation in whole rock Hf isotopes among the H-S samples likely indicates heterogeneity arising from establishment and evolution of the rift zone. Younger samples rhy6 and rhy7 from Phase 2 magmatism have slightly lower Hf isotope ratios more similar to that of basalt sample bas1, while Phase 1 silicic samples rhy2 and rhy3 are characterized by more radiogenic Hf. Therefore, it appears there is a component of isotopically distinct, more DM-like material contributing to the older Phase 1 magmas.

Two intriguing features of the Hf isotope data for H-S silicic samples are (1) an apparent discrepancy in some samples (rhy2, rhy3, and rhy6) between whole rock and in situ zircon Hf isotope compositions (Fig. 5c), and (2) variability in zircon ε_{Hf} in samples rhy2, rhy6, and grn1 as evidenced by high MSWD (Table 3). Whole rock ε_{Hf} is >1 epsilon unit

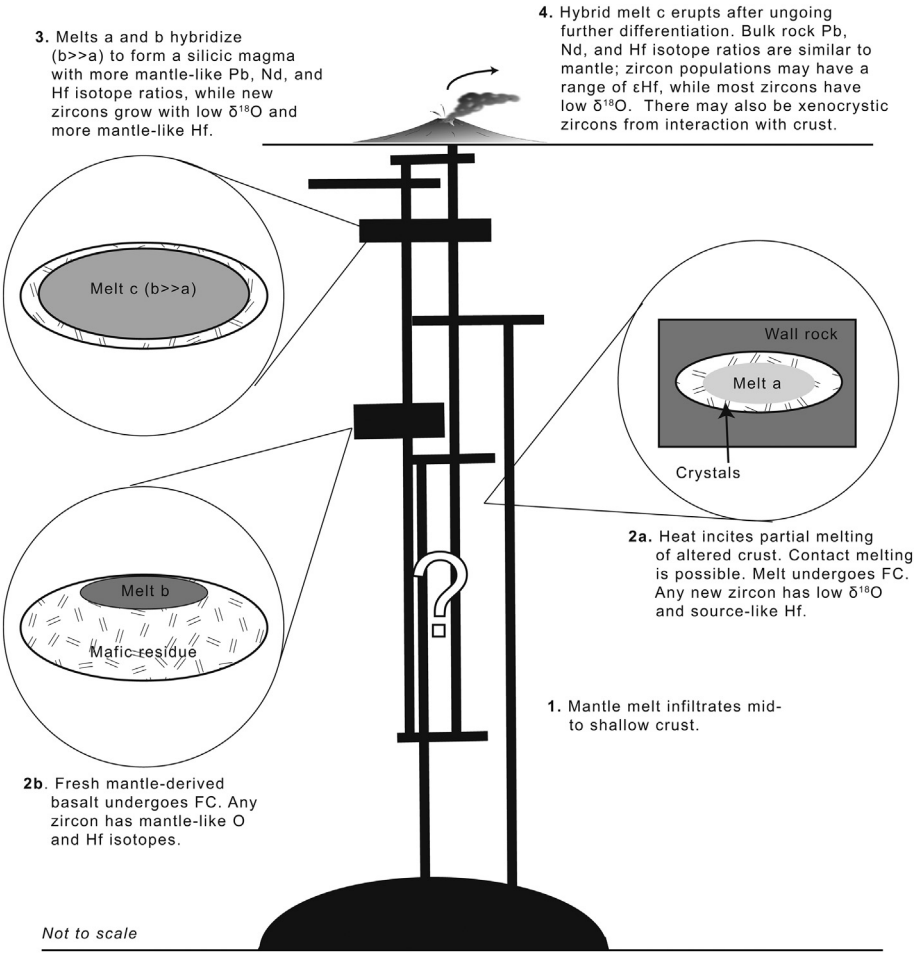

Fig. 7. Potential petrogenetic processes operating at Hafnarfjall-Skarðsheiði central volcano to produce silicic magmas that share whole-rock isotopic characteristics with co-genetic basalts but have zircon with low $\delta^{18}O$ and variable ε_{Hf}. No arrangement of magmatic plumbing system is implied. Figure is not to scale.

higher than the weighted average in situ zircon ε_{Hf} values in rhy2, rhy6, and grn1. Because Hf is extremely compatible in zircon but highly incompatible in the other H-S phenocryst phases, Hf not sequestered in zircon must primarily have resided in the melt. Discrepancies between whole rock and zircon ε_{Hf} thus indicate that the zircons grew in magmas that had different Hf isotopic compositions from those in which they were finally entrained, thus demonstrating magma evolution involving open-system processes.

Within-sample variation in Hf isotope composition, combined with statistical variability in analyses of secondary standards, supports the interpretation of natural intrasample variability. Secondary standard analyses were highly reproducible and yielded a range of ≤2 ε_{Hf} units. When typical errors are included, these analyses indicate that an expected range for a homogeneous population of zircon is ~4–5 epsilon units. This is the case for sample rhy7, for which zircon analyses fall within a narrow range (4 epsilon units, including error) and closely match the whole rock Hf isotope composition. Conversely, measured zircon Hf compositions in samples rhy2, rhy6, and grn1 have ranges of 4.5, 4.5, and 3.6 epsilon units. The spread in Hf isotope compositions among zircons within these samples indicates that zircon source magmas varied substantially in composition—that is, the erupted magmas represented mixtures of multiple zircon-bearing constituents.

Zircon ε_{Hf} from +8.3 to +13.7 in the H-S samples overlaps with but extends to considerably lower values than the range reported for basaltic magmas erupted from modern 'off-rift' zones and the propagating EVZ (ε_{Hf} ~ + 11 to +13.5). It is well below the range (ε_{Hf} ~ + 13.5 to +19) of modern established rifts (Peate et al., 2010).

5.3. Implications of zircon saturation and Ti-in-zircon thermometry

Temperatures suggested by saturation and Ti thermometry support the evidence from isotope data that suggests mixed sources of zircon crystals. Ti-in-zircon temperatures span ranges from 80 to 180 °C in individual samples, with only the higher temperatures approaching or exceeding the saturation temperatures. These low-T zircons (or zircon zones) are difficult to explain by growth in their host melt—this would require that they grew at a time when the magma was at relatively low temperature and crystal-rich, that the magma was subsequently intensely reheated, and that the low-T zircon failed to dissolve as temperature rose by up to 100–200 °C. Far more plausibly, many—and probably most—of the zircon crystals originally grew in other silicic magmas, in some cases in near-solidus magma chambers, and then were entrained in the ascending, ultimate host magma; quite likely, only a few of the zircon crystals are entirely native to the erupting magma. This is consistent with the clearly mixed oxygen isotopic populations of zircon in all samples, mixed Hf populations in at least some samples, and the hints of mixed U-Pb age populations.

5.4. Petrogenesis of silicic magmas and geodynamics at Hafnarfjall-Skarðsheiði

5.4.1. Petrogenesis of silicic magmas: a case for AFC processes

Hafnarfjall-Skarðsheiði volcano matured in a dynamic tectonic and magmatic setting at the nascent Western rift zone. Whole rock Pb, Nd, and Hf isotope data do not correlate with those from the

established Western rift zone, but instead with data from the modern propagating Eastern rift, suggesting that the rifting environment in which H-S magmas were produced was likely similar to that of the modern EVZ. Whole rock Pb, Nd, and Hf isotopic data from H-S basalt and silicic samples define coherent, tight groups, and thus they must be from source materials with the same small isotopic range. Whole rock radiogenic isotope signatures in H-S silicic and mafic magmas are ultimately derived from an enriched mantle source, as is currently the case in the EVZ (e.g. Peate et al., 2010); these data thus permit either fractional crystallization of mafic magma or anatexis of similarly-sourced mafic rock. Heterogeneity in zircon Hf and O isotope compositions lends support for an assimilation-fractional crystallization (AFC; DePaolo, 1981) petrogenesis. H-S zircons have low $\delta^{18}O$ values that indicate crystallization from isotopically light source magmas, and thus require assimilation of a fraction of hydrothermally altered bedrock into a melt derived from fractional crystallization of fresh mantle melt to explain the oxygen isotopic compositions. Sample rhy2 has an average $\delta^{18}O$ value of 2.2‰ that requires either lower $\delta^{18}O$ in the assimilant or the fractionated rhyolite or a higher assimilated fraction of bedrock. However, it seems unlikely that sufficient heat would be available to facilitate greater amounts of melting and assimilation during Phase 1 magmatism when the WRZ was likely less established than during Phase 2 magmatism; perhaps only small volumes could be dominated by the crustal signature with less heat. The rift zone crustal subsidence model of Pálmason (1973) suggests that bedrock temperatures under nascent H-S were < 600 °C at ~5 km depth—the depth that corresponds to the projected bedrock age of ~11 Myr based on the inherited core age in Pálmason (1973)'s model—which seems to preclude significant amounts of melting (Jónasson, 1994), at least until volumes of new injected basalt increase.

We summarize our preferred petrogenetic model for Hafnarfjall-Skarðsheiði silicic units as follows (Fig. 7):

1. Mantle-derived basalts dominated by the plume component infiltrate the mid-to-shallow crust
2. a. Heat from fresh basalt intrusions induces partial melting or assimilation of hydrothermally altered, low $\delta^{18}O$ crust, resulting in zircon with lower than mantle zircon $\delta^{18}O$ values and ε_{Hf} of the crustal source. b. Concurrently, fresh mantle-derived basalt dominated by the plume component undergoes fractional crystallization to produce rhyolite, which also saturates and crystallizes zircon with higher $\delta^{18}O$ values and ε_{Hf} values shared with the fresh mantle source.
3. Rhyolites produced in (2a) and (2b) hybridize and continue to crystallize zircon. Overall, the volume of (2b) is probably larger than (2a) based on oxygen isotopic data. Whole rock Pb, Nd, and Hf isotope compositions of basalt and rhyolite are similar. Lower zircon ε_{Hf} in some samples indicates a more enriched mantle origin, and probably reflects an anatectic component derived from a minor component of isotopically heterogeneous crust.
4. Eruption or emplacement occurs, with a hybrid magma composed of a proportion of FC-derived rhyolite mixed with a proportion of partial melt-derived rhyolite.

5.4.2. Geodynamic controls on petrogenesis

In situ zircon U-Pb ages indicate two distinct episodes of silicic magmatism at H-S: Phases 1 and 2, separated from each other by a gap of ~1 Myr during which only basalts erupted (Supplemental Table S6). Phase 1 magmatism was significantly shorter (perhaps 10s to ~100 kyr), while Phase 2 magmatism lasted ~500 kyr (including late-stage intrusions grn1 and gab1, which extend the volcanic record by 250 kyr). Franzson (1978) concluded that roughly 3–4% of Phase 1 magmas were rhyolitic, while later silicic units comprised 12–13% of the Phase 2 eruptive sequence. We contend that the magmatic phases, as well as the geochemical and isotope characteristics discussed above, can be integrated into a geodynamic model for petrogenesis of silicic units at Hafnarfjall-Skarðsheiði central volcano as follows (Fig. 8):

1. Pre-Phase 1 basalts erupted before the onset of silicic magmatism from the propagating/relocating WRZ.
2. Onset of silicic magmatism around 5.5 Myr, with a burst of Phase 1 silicic magmatism that lasted ~100 kyr from ~5.4 to 5.3 Ma. The geographic center of volcanism was in the north-central portion of the volcano near Brekkufjall (with the exception of rhy4, which is north of the volcano along a fissure). Silicic volcanism ceased when the volcano drifted too far from the rift axis to sustain thermal conditions conducive to eruption.
3. Basalts were the only evident magmatic products from ~5.3 to ~4.4 Ma.
4. Phase 2 silicic volcanism was active ~4.5–4.0 Ma. The locus of Phase 2 volcanism in the central-eastern region of the volcano was ~10 km from the locus of Phase 1 volcanism, normal to the rift axis.
5. Phase 2 silicic volcanism ended ~4.0 Ma because the plume head was far enough from the volcano that rift-supplied heat was insufficient to maintain silicic magma generation. The 3.9 Ma Flyðrur granophyre (sample grn1) is the youngest silicic unit at H-S.

Given the half-spreading rate of ~10 km/Myr (e.g. Thordarson and Höskuldsson, 2014), it seems clear that rift drift is responsible for the shift in location between Phase 1 and Phase 2 silicic magmas (Fig. 8), There is a ~1 Myr hiatus in silicic magma production between the two phases, which can be explained by rift drift—as can the distance between Phase 2 magmatism and the modern rift axis (~42 km). It should

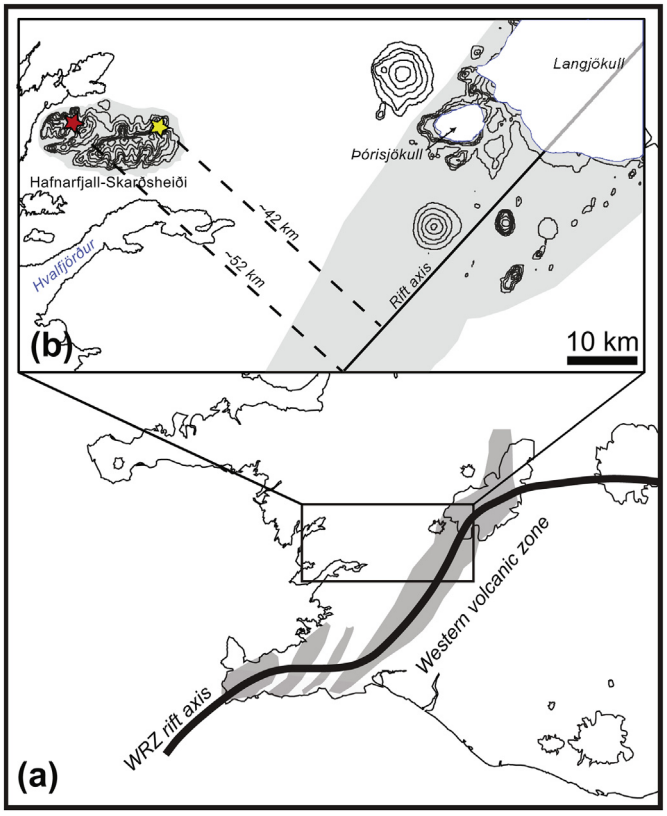

Fig. 8. Map of H—S demonstrating geodynamic evolution through the volcano's lifetime. (a) The Western volcanic zone (WVZ) with rift axis (after Harðarson et al. (2008)) demarcated by thick black line. (b) Distance between Phase 1 (red star) volcanism centered at rhy1 and Phase 2 (yellow star) volcanism centered at rhy7 and present center of rift axis is ~42 km, assuming perpendicular spreading. Centers of magmatism in Phases 1 and 2 are roughly 10 km apart.

be stressed that this general series of events could be duplicated at any central volcano that occupies a relatively uncomplicated tectonic area—that is, there are few major faults, no microplate boundaries, and no flank zones to interfere with rift drift's control over the timescales of magma production.

6. Conclusions

Silicic magmas produced at Hafnarfjall-Skarðsheiði central volcano in western Iceland between ~5.4 and ~3.9 Ma are the product of petrogenetic processes strongly influenced geochemically by fractionation of mantle-derived, plume-component-dominated basalt with modest assimilation of altered crust. This study provides a zircon-based view of petrogenesis in a single volcanic system that reveals: a) timescales of silicic magma production depend upon evolutionary stage on the source rift; b) generation of silicic magmas takes 10s to 100 s of kyr after a rift relocation; c) silicic systems may persist for >1.5 Myr, which is longer than many central volcanoes' lifetimes; and d) zircon isotopic data, coupled with whole rock isotope data, are critical to unravelling subtleties in source components, residence times, and petrogenesis. Our data indicate that silicic magmas at the long-lived Hafnarfjall-Skarðsheiði volcano are generated through fractionation of mantle-derived melts, in addition to melts derived from anatexis of hydrothermally altered, low $\delta^{18}O$ bedrock. This finding challenges alternate viewpoints invoking large-scale partial melting of altered crust for rhyolite generation in Iceland, and highlights the importance of multi-technique studies to further advance understanding of silicic crust generation processes in this unique geologic environment.

Supplementary data to this article can be found online at https://doi.org/10.1016/j.lithos.2018.08.022.

Acknowledgements

This work was funded primarily through a National Science Foundation grant (EAR1220523) to CFM. We thank A. Kerr, A. Gurenko, and M. Loewen for thoughtful reviews and comments that greatly improved this manuscript. Fieldwork was facilitated via a U.S. Fulbright Fellowship to Iceland to TJB, with invaluable suggestions from Á. Höskuldsson and H. Franzson. Thanks also to Áslaug and family for their hospitality during fieldwork; D. Wilford, C. Knaack, and R. Conrey for sample preparation and analysis at WSU; and A. Schmitt, R. Economos, and M-C. Liu for assistance at UCLA.

References

Baertschi, P., 1976. Absolute ^{18}O content of standard mean ocean water. Earth Planet. Sci. Lett. 31, 341–344.
Barboni, M., Boehnke, P., Schmitt, A.K., Harrison, T.M., Shane, P., Bouvier, A.-S., Baumgartner, L., 2016. Warm storage for arc magmas. Proc. Natl. Acad. Sci. 113, 13959–13964.
Benediktsdóttir, Á., Hey, R., Martinez, F., Höskuldsson, Á., 2012. Detailed tectonic evolution of the Reykjanes Ridge during the past 15 Ma. Geochem. Geophys. Geosyst. 13. https://doi.org/10.1029/2011GC003948.
Bindeman, I., 2008. Oxygen isotopes in mantle and crustal magmas as revealed by single crystal analysis. Rev. Mineral. Geochem. 69:445–478. https://doi.org/10.2138/rmg.2008.69.12.
Bindeman, I., Gurenko, A., Carley, T., Miller, C., Martin, E., Sigmarsson, O., 2012. Silicic magma petrogenesis in Iceland by remelting of hydrothermally altered crust based on oxygen isotope diversity and disequilibria between zircon and magma with implications for MORB. Terra Nova 24:227–232. https://doi.org/10.1111/j.1365-3121.2012.01058.x.
Bjarnason, I., 2008. An Iceland Hotspot Saga. Jökull 58, 1–16.
Black, L.P., Kamo, S.L., Allen, C.M., Davis, D.W., Aleinikoff, J.N., Valley, J.W., Mundil, R., Campbell, I.H., Korsch, R.J., Williams, I.S., Foudoulis, C., 2004. Improved 206Pb/238U microprobe geochronology by the monitoring of a trace-element-related matrix effect; SHRIMP, ID–TIMS, ELA–ICP–MS and oxygen isotope documentation for a series of zircon standards. Chem. Geol. 205, 115–140.
Boehnke, P., Watson, E.B., Trail, D., Harrison, T.M., Schmitt, A.K., 2013. Zircon saturation revisited. Chem. Geol. 351, 324–334.
Bouvier, A., Vervoort, J.D., Patchett, P.J., 2008. The Lu–Hf and Sm–Nd isotopic composition of CHUR: Constraints from unequilibrated chondrites and implications for the bulk composition of terrestrial planets. Earth Planet. Sci. Lett. 273, 48–57.
Brandsdóttir, B., Menke, W.H., 2008. The seismic structure of Iceland. Jökull 58, 17–34.
Browning, J., Gudmundsson, A., 2015. Caldera faults capture and deflect inclined sheets: an alternative mechanism of ring dike formation. Bull. Volcanol. 77, 4.
Carley, T.L., Miller, C.F., Wooden, J.L., Bindeman, I.N., Barth, A.P., 2011. Zircon from historic eruptions in Iceland: reconstructing storage and evolution of silicic magmas. Mineral. Petrol. 102, 135–161.
Carley, T.L., Miller, C.F., Wooden, J.L., Padilla, A.J., Schmitt, A.K., Economos, R.C., Bindeman, I.N., Jordan, B.T., 2014. Iceland is not a magmatic analog for the Hadean: Evidence from the zircon record. Earth Planet. Sci. Lett. 405, 85–97.
Carley, T.L., Miller, C.F., Sigmarsson, O., Coble, M.A., Fisher, C.M., Hanchar, J.M., Schmitt, A. K., Economos, R.C., 2017. Detrital zircon resolve longevity and evolution of silicic magmatism in extinct volcanic centers: A case study from the East Fjords of Iceland. Geosphere 13:1640–1663. https://doi.org/10.1130/GES01467.1.
Carmichael, I.S.E., 1964. The petrology of Thingmuli, a Tertiary volcano in eastern Iceland. J. Petrol. 5, 435–460.
Chauvel, C., Hémond, C., 2000. Melting of a complete section of recycled oceanic crust: trace element and Pb isotopic evidence from Iceland. Geochem. Geophys. Geosyst. 1. https://doi.org/10.1029/1999GC000002.
Claiborne, L.L., Miller, C.F., Flanagan, D.M., Clynne, M.A., Wooden, J.L., 2010. Zircon reveals protracted magma storage and recycling beneath Mount St. Helens. Geology 38, 1011–1014.
Claiborne, L.L., Miller, C.F., Gualda, G.A.R., Carley, T.L., Covey, A.K., Wooden, J.L., Fleming, M. A., 2018. Zircon as magma monitor: robust, temperature-dependent partition coefficients from glass and zircon surface and rim measurements from natural systems. In: Moser, D.E., Corfu, F., Darling, J.R., Reddy, S.M., Tait, K. (Eds.), Microstructural Geochronology: Planetary Records Down to Atom Scale. John Wiley & Sons, pp. 3–34.
DePaolo, D.J., 1981. Trace element and isotopic effects of combined wallrock assimilation and fractional crystallization. Earth Planet. Sci. Lett. 53, 189–202.
Ferry, J.M., Watson, E.B., 2007. New thermodynamic models and revised calibrations for the Ti-in-zircon and Zr-in-rutile thermometers. Contrib. Contrib. Mineral. Petrol. 154, 429–437.
Fisher, C.M., Hanchar, J.M., Samson, S.D., Dhuime, B., Blichert-Toft, J., Vervoort, J.D., Lam, R., 2011. Synthetic zircon doped with hafnium and rare earth elements: A reference material for in situ hafnium isotope analysis. Chem. Geol. 286:32–47. https://doi.org/10.1016/J.CHEMGEO.2011.04.013.
Fisher, C.M., Vervoort, J.D., DuFrane, S.A., 2014. Accurate Hf isotope determinations of complex zircons using the "laser ablation split stream" method. Geochem. Geophys. Geosyst. 15. https://doi.org/10.1002/2013GC004962.
Franzson, H., 1972. The Brekkufjall Caldera Formation, W. Iceland. University of St, Andrews.
Franzson, H., 1978. Structure and Petrochemistry of the Hafnarfjall-Skarðsheiði Central Volcano and the Surrounding Basalt Succession, W-Iceland. University of Edinburgh.
Furman, T., Frey, F.A., Meyer, P.S., 1992. Petrogenesis of Evolved Basalts and Rhyolites at Austurhorn, Southeastern Iceland: the Role of Fractional Crystallization. J. Petrol. 33, 1405–1445.
Furman, T., Frey, F., Park, K.-H., 1995. The scale of source heterogeneity beneath the Eastern neovolcanic zone, Iceland. J. Geol. Soc. Lond. 152:997–1002. https://doi.org/10.1144/GSL.JGS.1995.152.01.20.
Galer, S., Abouchami, W., 1998. Practical application of lead triple spiking for correction of instrumental mass discrimination. Mineral. Mag. 62A, 491–492.
Gautneb, H., Gudmundsson, A., Oskarsson, N., 1989. Structure, petrochemistry and evolution of a sheet swarm in an Icelandic central volcano. Geol. Mag. 126, 659–673.
Ghiorso, M.S., Gualda, G.A.R., 2013. A method for estimating the activity of titania in magmatic liquids from the compositions of coexisting rhombohedral and cubic iron–titanium oxides. Contrib. Mineral. Petrol. 165:73–81. https://doi.org/10.1007/s00410-012-0792-y.
Gunnarsson, B., Marsh, B.D., Taylor, H.P., 1998. Generation of Icelandic rhyolites: silicic lavas from the Torfajökull central volcano. J. Volcanol. Geotherm. Res. 83, 1–45.
Gurenko, A.A., Chaussidon, M., 2002. Oxygen isotope variations in primitive tholeiites of Iceland: evidence from a SIMS study of glass inclusions, olivine phenocrysts, and pillow rim glasses. Earth Planet. Sci. Lett. 205, 63–79.
Hanan, B.B., Graham, D.W., 1996. Lead and helium isotope evidence from oceanic basalts for a common deep source of mantle plumes. Science 272, 991–995.
Hanan, B.B., Schilling, J.-G., 1997. The dynamic evolution of the Iceland mantle plume: the lead isotope perspective. Earth Planet. Sci. Lett. 151:43–60. https://doi.org/10.1016/S0012-821X(97)00105-2.
Hardarson, B.S., Fitton, J.G., Ellam, R.M., Pringle, M.S., 1997. Rift relocation — a geochemical and geochronological investigation of a palaeo-rift in northwest Iceland. Earth Planet. Sci. Lett. 153:181–196. https://doi.org/10.1016/S0012-821X(97)00145-3.
Harðarson, B.S., Fitton, J.G., Hjartarson, Á., 2008. Tertiary volcanism in Iceland. Jökull 58, 161–178.
Hart, S.R., 1984. A large-scale isotope anomaly in the Southern Hemisphere mantle. Nature 309, 753–757.
Hart, S.R., Hauri, E.H., Oschmann, L.A., Whitehead, J.A., 1992. Mantle plumes and entrainment: isotopic evidence. Science 256:517–520. https://doi.org/10.1126/science.256.5056.517.
Hattori, K., Muehlenbachs, K., 1982. Oxygen isotope ratios of the Icelandic crust. J. Geophys. Res. 87, 6559–6565.
Hemond, C., Arndt, N.T., Lichtenstein, U., Hofmann, A.W., Oskarsson, N., Steinthorsson, S., 1993. The heterogeneous Iceland plume: Nd-Sr-O isotopes and trace element constraints. J. Geophys. Res. 98:15833. https://doi.org/10.1029/93JB01093.
Hilton, D.R., Grönvold, K., Macpherson, C.G., Castillo, P.R., 1999. Extreme 3He/4He ratios in northwest Iceland: constraining the common component in mantle plumes. Earth Planet. Sci. Lett. 173:53–60. https://doi.org/10.1016/S0012-821X(99)00215-0.
Hoskin, P.W.O., Schaltegger, U., 2003. The Composition of Zircon and Igneous and Metamorphic Petrogenesis. Rev. Mineral. Geochem. 53, 27–62.

Jóhannesson, H., 1980. Evolution of rift zones in western Iceland. Náttúrufræðingurinn 50, 13–31.
Johnson, D., Hooper, P., Conrey, R., 1999. XRF analysis of rocks and minerals for major and trace elements on a single low dilution Li-tetraborate fused bead. Adv. X-ray Anal. 41, 843–867.
Jónasson, K., 1994. Rhyolite volcanism in the Krafla central volcano, north-east Iceland. Bull. Volcanol. 56, 516–528.
Jónasson, K., 2007. Silicic volcanism in Iceland: Composition and distribution within the active volcanic zones. J. Geodyn. 43, 101–117.
Kitagawa, H., Kobayashi, K., Makishima, A., Nakamura, E., 2008. Multiple pulses of the mantle Plume: Evidence from tertiary Icelandic lavas. J. Petrol. 49, 1365–1396.
Kokfelt, T.F., Hoernle, K., Hauff, F., Fiebig, J., Werner, R., Garbe-Schönberg, D., 2006. Combined trace element and Pb-Nd-Sr-O isotope evidence for recycled oceanic crust (upper and lower) in the Iceland mantle plume. J. Petrol. 47:1705–1749. https://doi.org/10.1093/petrology/egl025.
Ludwig, K.R., 2009. SQUID 2, A User's Manual. 100. Berkeley Geochronol. Cent. Spec. Publ.
Ludwig, K.R., 2012. Isoplot 3.75, A Geochronological Toolkit for Excel. 75. Berkeley Geochronology Center Special Publication.
Lugmair, G.W., Shimamura, T., Lewis, R.S., Anders, E., 1983. Samarium-146 in the early solar system: evidence from neodymium in the Allende meteorite. Science 222, 1015–1018.
Macdonald, R., Sparks, R.S.J., Sigurdsson, H., Mattey, D.P., McGarvie, D.W., Smith, R.L., 1987. The 1875 eruption of Askja volcano, Iceland: combined fractional crystallization and selective contamination in the generation of rhyolitic magma. Mineral. Mag. 51, 183–202.
Mahon, K.I., 1996. The New "York" regression: application of an improved statistical method to geochemistry. Int. Geol. Rev. 38, 293–303.
Marsh, B.D., Gunnarsson, B., Congdon, R., Carmody, R., 1991. Hawaiian basalt and Icelandic rhyolite: indicators of differentiation and partial melting. Geol. Rundsch. 80, 481–510.
Martin, E., Sigmarsson, O., 2007. Crustal thermal state and origin of silicic magma in Iceland: the case of Torfajökull, Ljósufjöll and Snæfellsjökull volcanoes. Contrib. Mineral. Petrol. 153, 593–605.
Martin, E., Sigmarsson, O., 2010. Thirteen million years of silicic magma production in Iceland: Links between petrogenesis and tectonic settings. Lithos 116, 129–144.
Martin, E., Martin, H., Sigmarsson, O., 2008. Could Iceland be a modern analogue for the Earth's early continental crust? Terra Nova 20, 463–468.
Martin, E., Paquette, J.L., Bosse, V., Ruffet, G., Tiepolo, M., Sigmarsson, O., 2011. Geodynamics of rift–plume interaction in Iceland as constrained by new $^{40}Ar/^{39}Ar$ and in situ U–Pb zircon ages. Earth Planet. Sci. Lett. 311, 28–38.
McDonough, W.F., Sun, S.-S., 1995. The composition of the Earth. Chem. Geol. 120, 223–253.
McDowell, S.M., Overton, S., Fisher, C.M., Frazier, W.O., Miller, C.F., Miller, J.S., Economos, R.C., 2016. Hafnium, oxygen, neodymium, strontium, and lead isotopic constraints on magmatic evolution of the supereruptive southern Black Mountains volcanic center, Arizona, USA: A combined LASS zircon–whole-rock study. Am. Mineral. 101, 311–327.
Mertz, D.F., Haase, K.M., 1997. The radiogenic isotope composition of the high-latitude North Atlantic mantle. Geology 25:411. https://doi.org/10.1130/0091-7613(1997)025<0411:TRICOT>2.3.CO;2.
Moorbath, S., Sigurdsson, H., Goodwin, R., 1968. K-Ar ages of the oldest exposed rocks in Iceland. Earth Planet. Sci. Lett. 4, 197–205.
Morel, M.L.A., Nebel, O., Nebel-Jacobsen, Y.J., Miller, J.S., Vroon, P.Z., 2008. Hafnium isotope characterization of the GJ-1 zircon reference material by solution and laser-ablation MC-ICPMS. Chem. Geol. 255:231–235. https://doi.org/10.1016/j.chemgeo.2008.06.040.
Muehlenbachs, K., Anderson, A.T., Sigvaldason, G.E., 1974. Low-O^{18} basalts from Iceland. Geochim. Cosmochim. Acta 38, 577–588.
Nicholson, H., Condomines, M., Fitton, J.G., Fallick, A.E., Grönvold, K., Rogers, G., 1991. Geochemical and isotopic evidence for crustal assimilation beneath Krafla, Iceland. J. Petrol. 32, 1005–1020.
Óskarsson, N., Sigvaldason, G.E., Steinthorsson, S., 1982. A dynamic model of rift zone petrogenesis and the regional petrology of Iceland. J. Petrol. 23, 28–74.
Óskarsson, N., Steinthórsson, S., Sigvaldason, G.E., 1985. Iceland geochemical anomaly: Origin, volcanotectonics, chemical fractionation and isotope evolution of the crust. J. Geophys. Res. 90:10011–10025. https://doi.org/10.1029/JB090iB12p10011.
Padilla, A.J., Miller, C.F., Carley, T.L., Economos, R.C., Schmitt, A.K., Coble, M.A., Wooden, J.L., Fisher, C.M., Vervoort, J.D., Hanchar, J.M., 2016. Elucidating the magmatic history of the Austurhorn silicic intrusive complex (southeast Iceland) using zircon elemental and isotopic geochemistry and geochronology. Contrib. Mineral. Petrol. 171:69. https://doi.org/10.1007/s00410-016-1279-z.
Pálmason, G., 1973. Kinematics and heat flow in a volcanic rift zone, with application to Iceland. Geophys. J. Int. 33, 451–481.
Peate, D.W., Breddam, K., Baker, J.A., Kurz, M.D., Barker, A.K., Prestvik, T., Grassineau, N., Skovgaard, A.C., 2010. Compositional characteristics and spatial distribution of enriched Icelandic mantle components. J. Petrol. 51, 1447–1475.
Pope, E.C., Bird, D.K., Arnórsson, S., 2013. Evolution of low-^{18}O Icelandic crust. Earth Planet. Sci. Lett. 374, 47–59.
Prestvik, T., Goldberg, S., Karlsson, H., Grönvold, K., 2001. Anomalous strontium and lead isotope signatures in the off-rift Öræfajökull central volcano in south-east Iceland: Evidence for enriched endmember(s) of the Iceland mantle plume? Earth Planet. Sci. Lett. 190, 211–220.
Reimink, J.R., Chacko, T., Stern, R.A., Heaman, L.M., 2014. Earth's earliest evolved crust generated in an Iceland-like setting. Nat. Geosci. 7, 529–533.
Sæmundsson, K., 1967. An outline of the structure of SW-Iceland. In: Björnsson, S. (Ed.), Iceland and Mid-Ocean Ridges. Society Scientifica Islandica, Rit 38, Reykjavík, Iceland.
Sæmundsson, K., 1974. Evolution of the axial rifting zone in northern Iceland and the Tjörnes fracture zone. GSA Bull. 85, 465–504.
Sæmundsson, K., 1986. Subaerial volcanism in the western North Atlantic. In: Vogt, P.R., Tucholke, B.E. (Eds.), The Geology of North America. The Western North Atlantic Region vol. M. Geological Society of America, Boulder, CO, pp. 69–86.
Schärer, U., 1984. The effect of initial230Th disequilibrium on young UPb ages: the Makalu case, Himalaya. Earth Planet. Sci. Lett. 67:191–204. https://doi.org/10.1016/0012-821X(84)90114-6.
Schmitt, A.K., Stockli, D.F., Lindsay, J.M., Robertson, R., Lovera, O.M., Kislitsyn, R., 2010. Episodic growth and homogenization of plutonic roots in arc volcanoes from combined U–Th and (U–Th)/He zircon dating. Earth Planet. Sci. Lett. 295, 91–103.
Shorttle, O., Maclennan, J., Piotrowski, A.M., 2013. Geochemical provincialism in the Iceland plume. Geochim. Cosmochim. Acta 122:363–397. https://doi.org/10.1016/J.GCA.2013.08.032.
Sigmarsson, O., Steinthórsson, S., 2007. Origin of Icelandic basalts: A review of their petrology and geochemistry. J. Geodyn. 43:87–100. https://doi.org/10.1016/J.JOG.2006.09.016.
Sigmarsson, O., Hemond, C., Condomines, M., Fourcade, S., Oskarsson, N., 1991. Origin of silicic magma in Iceland revealed by Th isotopes. Geology 19, 621–624.
Sigmarsson, O., Condomines, M., Fourcade, S., 1992a. A detailed Th, Sr and O isotope study of Hekla: differentiation processes in an Icelandic volcano. Contrib. Mineral. Petrol. 112, 20–34.
Sigmarsson, O., Condomines, M., Fourcade, S., 1992b. Mantle and crustal contribution in the genesis of Recent basalts from off-rift zones in Iceland: Constraints from Th, Sr and O isotopes. Earth Planet. Sci. Lett. 110:149–162. https://doi.org/10.1016/0012-821X(92)90045-W.
Sigmarsson, O., Maclennan, J., Carpentier, M., 2008. Geochemistry of igenous rocks in Iceland: a review. Jökull 58, 139–160.
Stacey, J.S., Kramers, J.D., 1975. Approximation of terrestrial lead isotope evolution by a two-stage model. Earth Planet. Sci. Lett. 26, 207–221.
Stecher, O., Carlson, R.W., Gunnarsson, B., 1999. Torfajökull: a radiogenic end-member of the Iceland Pb-isotopic array. Earth Planet. Sci. Lett. 165:117–127. https://doi.org/10.1016/S0012-821X(98)00256-8.
Thirlwall, M.F., Gee, M.A.M., Taylor, R.N., Murton, B.J., 2004. Mantle components in Iceland and adjacent ridges investigated using double-spike Pb isotope ratios. Geochim. Cosmochim. Acta 68, 361–386.
Thirlwall, M.F., Gee, M.A.M., Lowry, D., Mattey, D.P., Murton, B.J., Taylor, R.N., 2006. Low δ18O in the Icelandic mantle and its origins: Evidence from Reykjanes Ridge and Icelandic lavas. Geochim. Cosmochim. Acta 70, 993–1019.
Thorarinsson, S., 1967. Hekla and Katla: The share of acid and intermediate lava and tephra in the volcanic products through the geological history of Iceland. Soc. Sci. Islandica 38, 190–199.
Thordarson, T., Höskuldsson, Á., 2014. Classic Geology in Europe 3: Iceland. 2nd ed. Dunedin Academic Press, Edinburgh.
Torsvik, T.H., Amundsen, H.E.F., Tronnes, R.G., Doubrovine, P.V., Gaina, C., Kusznir, N.J., Steinberger, B., Corfu, F., Ashwal, L.D., Griffin, W.L., Werner, S.C., Jamtveit, B., 2015. Continental crust beneath southeast Iceland. Proc. Natl. Acad. Sci. E1818–E1827.
Trail, D., Mojzsis, S.J., Harrison, T.M., Schmitt, A.K., Watson, E.B., Young, E.D., 2007. Constraints on Hadean zircon protoliths from oxygen isotopes, Ti-thermometry, and rare earth elements. Geochem. Geophys. Geosyst. 8.
Trail, D., Bindeman, I.N., Watson, E.B., Schmitt, A.K., 2009. Experimental calibration of oxygen isotope fractionation between quartz and zircon. Geochim. Cosmochim. Acta 73:7110–7126. https://doi.org/10.1016/J.GCA.2009.08.024.
Valley, J.W., 2003. Oxygen Isotopes in Zircon. Rev. Mineral. Geochem. 53, 343–385.
Valley, J.W., Kinny, P.D., Schulze, D.J., Spicuzza, M.J., 1998. Zircon megacrysts from kimberlite: oxygen isotope variability among mantle melts. Contrib. Mineral. Petrol. 133, 1–11.
Valley, J.W., Lackey, J.S., Cavosie, A.J., Clechenko, C.C., Spicuzza, M.J., Basei, M.A.S., Bindeman, I.N., Ferreira, V.P., Sial, A.N., King, E.M., Peck, W.H., Sinha, A.K., Wei, C.S., 2005. 4.4 billion years of crustal maturation: oxygen isotope ratios of magmatic zircon. Contrib. Mineral. Petrol. 150, 561–580.
Vervoort, J.D., Blichert-Toft, J., 1999. Evolution of the depleted mantle: Hf isotope evidence from juvenile rocks through time. Geochim. Cosmochim. Acta 63:533–556. https://doi.org/10.1016/S0016-7037(98)00274-9.
Vink, G.E., 1984. A hotspot model for Iceland and the Vøring Plateau. J. Geophys. Res. 89, 9949–9959.
Walker, G.P.L., 1966. Acid rocks in Iceland. Bull. Volcanol. 29, 375–402.
Watson, E.B., Harrison, T.M., 1983. Zircon saturation revisited: temperature and composition effects in a variety of crustal magma types. Earth Planet. Sci. Lett. 64, 295–304.
Watson, E.B., Wark, D.A., Thomas, J.B., 2006. Crystallization thermometers for zircon and rutile. Contrib. Mineral. Petrol. 151, 413–433.
Willbold, M., Hegner, E., Stracke, A., Rocholl, A., 2009. Continental geochemical signatures in dacites from Iceland and implications for models of early Archaean crust formation. Earth Planet. Sci. Lett. 279, 44–52.
Woodhead, J.D., Hergt, J.M., 2005. A preliminary appraisal of seven natural zircon reference materials for in Situ Hf isotope determination. Geostand. Geoanal. Res. 29, 183–195.
Zindler, A., Hart, S., 1986. Chemical geodynamics. Annu. Rev. Earth Planet. Sci. 14, 493–571.